NTNU
Innovation and Creativity

Robust control of ROV/AUVs

Eirik Svendby

Master of Science in Engineering Cybernetics
Submission date: June 2007
Supervisor: Kristin Ytterstad Pettersen, ITK

Norwegian University of Science and Technology
Department of Engineering Cybernetics

Problem Description

The purpose of this project is to develop and implement a control system for ROV Minerva. ROV Minerva is currently manually controlled by an operator. In order to improve the performance of survey operations, a closed-loop control system must be developed for the ROV.

1. Develop a full 6DOF modell of ROV Minerva, including the cable drag force.

2. Develop a controller for pitch and roll control, estimating and compensating for the cable force.

3. Develop a control system that makes Minerva follow a lawn-mower system at the same time as it keeps a constant distance from the sea bed. ROV Minerva is equipped with 4 sonars that measure the distance to the seabed. The assignment is to develop a system that lets the ROV keep a constant distance to the seabed, while following, in turn, a set of parallel lines in the horizontal plane. The purpose is to get a visual mapping of the seabed. The control system should preferably be robust to model parameter errors and influence from currents.

4. Verify the theoretical results by simulations and experiments, doing a back-to-back comparison between simulation and experimental results.

5. (Possibly) consider the case where the lateral thruster fails/the ROV/AUV has the typical thruster configuration of AUVs without lateral thrusters.

Assignment given: 08. January 2007
Supervisor: Kristin Ytterstad Pettersen, ITK

Preface

This report represents my master thesis, and presents the work done during the tenth semester of my study for the M.Sc. degree in Engineering Cybernetics at the Norwegian University of Science and Technology (NTNU).

I would like to thank advisors Professor Kristin Ytterstad Pettersen and Dr. Alexey Pavlov, and co-advisors Even Børhaug, Dr. Erik Kyrkjebø and Martin Ludvigsen for their help and guidance. I would also like to thank Jesper Nordgård for his help with the communication protocol of ROV Minerva.

Eirik Svendby

Trondheim, 1. June 2007

Abstract

In this project a robust adaptive controller has been developed for Minerva, NTNU's research ROV. The controller was tested in simulation using Matlab/Simulink with a mathematical model of the vessel. It was also tested in a practical experiment at sea, with the ROV Minerva.

The simulations, the control system performs very well. The results from the practical experiment are promising, but several improvements are necessary before the system works satisfactory. The single factor which is believed to degrade the perfomance the most is an error in the mapping between thrust force and rotational speed.

Contents

1 Introduction **1**

1.1 The ROV Minerva 1

1.2 Project Objectives 1

2 Modelling **3**

2.1 Kinematics 3

2.1.1 Degrees of Freedom 3

2.1.2 Reference Frames 3

2.2 Dynamics 5

2.2.1 System Inertia 5

2.2.2 Damping 6

2.2.3 Gravitational and Bouyancy Forces and Moments 6

2.2.4 Cable Drag 7

3 Control Theory **9**

3.1 The Adaptive Controller 9

3.1.1 Nonlinear Model-Reference Adaptive Control 10

3.1.2 Robustness 11

4 Simulation **13**

4.1 Implementation 13

4.1.1 Guidance 13

4.2 Simulation 15
4.2.1 The Vessel Model 17
4.2.2 Simulation Results 19

5 Practical Experiments **23**
5.1 Implementation 23
5.1.1 Communication and Real-Time Execution 23
5.1.2 Control Allocation 24
5.1.3 Mapping between Thrust Force and Rotational Speed . . 26
5.1.4 Measurements 27
5.1.5 Settings 27
5.2 Results 29

6 Discussion **39**

7 Conclusions **41**

8 Further Work **43**

A Simulation Plots **45**

B Plots from Experiments **65**

C Simulator in Matlab/Simulink **77**

List of Figures

4.1 The path travelled in the xy-plane 19

4.2 η as a function of time 20

4.3 $\tilde{\eta}$ as a function of time 21

4.4 $\tilde{\eta}$ as a function of time with reduced damping in yaw 22

5.1 Thruster configuration of ROV Minerva, view from top (Courtesy of M. Ludvigsen) 31

5.2 Thruster configuration of ROV Minerva, view from side (Courtesy of M. Ludvigsen) 32

5.3 η as a function of time 33

5.4 $\tilde{\eta}$ as a function of time 34

5.5 ν as a function of time 35

5.6 RPM of thrusters as a function of time 36

5.7 Diagonal elements of estimated system inertia matrix as functions of time 37

5.8 Diagonal elements of estimated linear damping matrix as functions of time 38

A.1 ν as a function of time 45

A.2 $\tilde{\nu}$ as a function of time 46

A.3 τ as a function of time 47

A.4 First row of estimated system inertia matrix 48

A.5 Second row of estimated system inertia matrix 49

A.6 Third row of estimated system inertia matrix 50

A.7 Fourth row of estimated system inertia matrix 51
A.8 Fifth row of estimated system inertia matrix 52
A.9 Sixth row of estimated system inertia matrix 53
A.10 First row of estimated linear damping matrix 54
A.11 Second row of estimated linear damping matrix 55
A.12 Third row of estimated linear damping matrix 56
A.13 Fourth row of estimated linear damping matrix 57
A.14 Fifth row of estimated linear damping matrix 58
A.15 Sixth row of estimated linear damping matrix 59
A.16 The estimated quadratic damping matrix 60
A.17 The estimated environmental disturbance 61
A.18 The estimated spring constant from the cable 62
A.19 The estimated gravitational/bouyancy force 63

B.1 First row of estimated system inertia matrix as functions of time 65
B.2 Second row of estimated system inertia matrix as functions of time 66
B.3 Third row of estimated system inertia matrix as functions of time 67
B.4 Sixth row of estimated system inertia matrix as functions of time 68
B.5 First row of estimated linear damping matrix as functions of time 69
B.6 Second row of estimated linear damping matrix as functions of time 70
B.7 Third row of estimated linear damping matrix as functions of time 71
B.8 Sixth row of estimated linear damping matrix as functions of time 72
B.9 Diagonal elements of estimated quadratic damping matrix as functions of time 73
B.10 Estimated environmental disturbance as a function of time . . . 74
B.11 Estimated gravity/bouyancy parameters as functions of time . . 75

Chapter 1

Introduction

This project is a continuation of the work done in (Svendby, 2006), where a robust adaptive control system for the ROV Minerva was developed. Four degrees of freedom were controlled, surge, sway, heave and yaw.

1.1 The ROV Minerva

The ROV is a SUB-Fighter 7500 from Sperre AS. It has five thrusters, two vertical, one lateral and two forward thrusters. An umbilical cable is used for communication between the ROV and the mother ship, R/V Gunnerus.

ROV Minerva is at present only controlled directly by an operator. The project wishes to augment the ROV with a path following control system.

The hydrodynamic parameters of the mathematical model of the ROV are uncertain. They will also be altered when the ROV is mounted with different equipment, including lights and cameras. When at great depths, the ROV may experience compression. This will change the parameters. Because of the factors stated here, it has been decided that the controller shall be an adaptive one.

1.2 Project Objectives

A control system for the remotely operated underwater vehicle, ROV Minerva, shall be developed. All six degrees of freedom will be controlled, and cable drag will be accounted for.

A simulator shall be implemented in Matlab/Simulink, based on the available data from the ROV. Theoretical results should be validated through simulations using the simulator, and experiments with the ROV Minerva.

Chapter 2

Modelling

2.1 Kinematics

2.1.1 Degrees of Freedom

The ROV Minerva is assumed to be a rigid body. In order to describe the motion of a rigid body in space the SNAME definition with six degrees of freedom (DOF) is used. The first three DOF describe the position and translational motion of the body, while the last three DOF describe the orientation in space and the rotational motion. The standard definition of the DOF of marine vessels is presented in table 2.1 (Fossen, 2002).

Table 2.1: DOF notation for marine vessels

DOF		Velocities	Positions and Euler angles
1	motions in the x-direction (surge)	u	x
2	motions in the y-direction (sway)	v	y
3	motions in the z-direction (heave)	w	z
4	rotation about the x-axis (roll)	p	ϕ
5	rotation about the y-axis (pitch)	q	θ
6	rotation about the z-axis (yaw)	r	ψ

2.1.2 Reference Frames

Two reference frames are utilised in this project; the n-frame and the b-frame described in (Fossen, 2002). The vessel will only operate inside a small geographical area, which means that one can assume the Earth to be flat for

this operating area. The origin of the n-frame is is fixed to some point on the tangent plane of the surface of the Earth. The x-axis points towards north, the y-axis points towards east, and the z-axis points downwards, normal to the tangent plane.

The b-frame is also known as the BODY-frame. The x-axis points ahead, the y-axis points starboard, and the z-axis points downwards, normal to the xy-plane

Vectorial Representation

In this report two vectors will be used to represent position, orientation and velocity. Position and orientation is given in the n-frame by:

$$\eta = \begin{bmatrix} x \\ y \\ z \\ \phi \\ \theta \\ \psi \end{bmatrix}$$

Translational and angular velocity is given in the b-frame by:

$$\nu = \begin{bmatrix} u \\ v \\ w \\ p \\ q \\ r \end{bmatrix}$$

Transformation between frames

The standard transformation matrix for 6 DOF is used to express the relation:

$$\dot{\eta} = J(\Theta)\nu \tag{2.1}$$

Θ is the vector that describes the orientation of the vessel, that is:

$$\mathbf{\Theta} = \begin{bmatrix} \phi \\ \theta \\ \psi \end{bmatrix}$$

The expression for the transformation matrix is found in (Fossen, 2002).

2.2 Dynamics

In order to synthesise the controller, a mathematical model describing the dynamics of the ROV Minerva is needed. An extended version of the model used in (Svendby, 2006) will be used. The model is based on the general model for marine vessels presented in (Fossen, 2002). There one can find methods for determining the rigid body inertia matrix and the vector of gravitational/bouyancy forces and moments.

$$M\dot{\nu} + D(\nu)\nu + K_{cd}(\eta - \eta_{cd}) + g(\eta) = \tau + w \tag{2.2}$$

where

M	- system inertia matrix
$D(\nu)$	- damping matrix
$g(\eta)$	- vector of gravitational/buoyancy forces and moments
K_{cd}	- cable drag matrix
τ	- vector of control inputs
w	- vector of environmental disturbances
η_{cd}	- position of umbilical end point.

This model is the standard model for a 6 DOF vessel with position mooring, and disregarding the Coriolis and centripetal forces. These forces can be disregarded because the vessel will operate at low speeds, rendering the Coriolis and centripetal forces negligible.

For position mooring a spring model is used. For this specific vessel this spring model will be used to describe the effect of cable drag from the umbilical.

2.2.1 System Inertia

The system inertia matrix is a sum of the rigid body inertia matrix and the added mass inertia matrix. The former is possible to find analytically using knowledge of the geometry of the vessel (see (Fossen, 2002)), but the latter is difficult to determine.

2.2.2 Damping

The $D(\nu)$ matrix represents the hydrodynamic damping, with contributions from several damping phenomena. It can be represented as a sum of the linear and the quadratic damping (Fossen, 2002):

$$D(\nu) = D_l + D_q\nu \tag{2.3}$$

These damping matrices contribute significantly to the behaviour of the vessel. They are also difficult to determine, both analytically and empirically. These factors justify the use of an adaptive controller.

When implementing the controller, only the diagonal elements of the quadratic damping matrix are assumed to be important. The off-diagonal elements are assumed to be negligible because of the low speed at which the vessel operates.

2.2.3 Gravitational and Bouyancy Forces and Moments

The forces and moments due to gravity and bouyancy are represented by the vector:

$$\mathbf{g}(\eta) = \begin{bmatrix} (W-B)\sin\theta \\ -(W-B)\cos\theta\sin\phi \\ -(W-B)\cos\theta\cos\phi \\ -(y_gW - y_bB)\cos\theta\cos\phi + (z_gW - z_bB)\cos\theta\sin\phi \\ (z_gW - z_bB)\sin\theta + (x_gW - x_bB)\cos\theta\cos\phi \\ -(x_gW - x_bB)\cos\theta\sin\phi - (y_gW - y_bB)\sin\theta \end{bmatrix}$$

where W is the force of gravity on the vessel, B is the bouyancy force, and

$$\mathbf{r_g} = \begin{bmatrix} x_g \\ y_g \\ z_g \end{bmatrix}$$

and

$$\mathbf{r_b} = \begin{bmatrix} x_b \\ y_b \\ z_b \end{bmatrix}$$

are the vectors describing the distance of the origin from the centre of gravity and the centre of bouyancy, respectively.

2.2.4 Cable Drag

The ROV Minerva is attached to an umbilical cable which provides it with power and control signals, and communicates measurement signals from the ROV to the mother ship. This cable will impose forces on the ROV due to drag.

There are several ways to model the cable drag. One approach is to model the cable as several lumped masses attached to eachother through springs. The number of lumped masses is dynamic, as it depends on the length of the cable. For this reason implementation is complicated. Due to its simplicity, a mass-spring-damper system is used to model the vessel with umbilical.

The umbilical adds both spring and damping effects. The spring effects are modelled as position mooring in the standard model of (Fossen, 2002). The spring constant matrix is assumed to be a diagonal matrix.

Chapter 3

Control Theory

3.1 The Adaptive Controller

Motivated by the uncertainties of the parameters in equation 2.2, the controller will be adaptive. This signifies that in the control law the uncertain or varying parameters are represented by adjustable parameters. An adaptive law governs the adjustment of these parameters.

According to (Slotine and Li, 1991) and (Ioannou and Sun, 1996) there are two main approaches to adaptive control. These are the model-reference adaptive control method (MRAC) and the self-tuning method. The latter method focuses on estimation of the unknown parameters. These estimates are then used to determine the controller parameters, using a conventional technique, for example pole placement. The drawback of this approach is that it requires parameter estimate convergence in order to ensure stability. In fact, the parameter estimates will only converge to the true parameter values if the reference signal satisfies certain conditions; the signal has to be persistently exciting.

The parameter convergence requirement, and the requirements of the reference signal to ensure this convergence, means that a complex initialisation routine is necessary. This is highly undesirable because designing such a routine is not a trivial task, and performing it raises the threshold for using the ROV.

The MRAC method, on the other hand, guarantees convergence to the desired path. The parameter estimates will adapt so as to follow the desired path, and will not preoccupy with converging to the true parameter values. It is of course possible that they converge to the true values, but only if the condition of persistently exciting reference signals is satisfied.

The ability of the model-reference adaptive control method to let the vessel

start its path following right away, makes it a good choice for the application in this project.

3.1.1 Nonlinear Model-Reference Adaptive Control

Both (Slotine and Li, 1991) and (Fossen, 2002) suggest equivalent model-reference adaptive control schemes for nonlinear systems. The latter will be implemented in this project, and is presented here.

Based on the vessel dynamics equation, the control law is:

$$\tau = \hat{M}a^b + \hat{D}_l\nu + \hat{D}_q\left|\nu\right|\nu + \hat{K}_c d(\eta - \eta_{cd}) + \hat{g}(\eta) - \hat{w} \tag{3.1}$$

The hat means that the parameters are estimates, and a^b is the commanded acceleration, decomposed in the b-frame. The commanded acceleration, decomposed in the n-frame, is defined as:

$$a^n = \ddot{\eta}_d - K_d\dot{\tilde{\eta}} - K_p\tilde{\eta} \tag{3.2}$$

where η_d is the desired position,

$$\tilde{\eta} = \eta - \eta_d \tag{3.3}$$

and the dot denotes the derivative.

The left-hand side of equation 3.1 is parameterised so that:

$$\tau = \Phi(a^b, \nu, \eta)\hat{\theta} \tag{3.4}$$

θ is a vector of the unknown matrix parameters and $\hat{\theta}$ is the estimate of it, while $\Phi(a^b, \nu, \eta)$ is a matrix that contains the variables. These are measured and hence known.

The parameter adaptation law used to update the parameter vector is:

$$\dot{\hat{\theta}} = -\Gamma\Phi^T(a^b, \nu, \eta)J^{-1}s \tag{3.5}$$

where the combined error is defined as

$$s = \dot{\tilde{\eta}} + \lambda_0\tilde{\eta} \tag{3.6}$$

, λ_0 is a positive constant and $\Gamma = \Gamma^T > 0$ is the adaptation gain matrix.

The resulting error dynamics are then:

$$M[\dot{\nu} - a^b] = [\hat{M} - M]a^b + \tilde{D}_l\nu + \tilde{D}_q\left|\nu\right|\nu + \tilde{K}_c d(\eta - \eta_{cd}) + \tilde{g}(\eta) - \tilde{w} \tag{3.7}$$

Parameterising the right-hand side and transforming the left-hand side to the n-frame yields:

$$MJ^{-1}(\eta)[\ddot{\eta} - a^n] = \Phi(a^b, \nu, \eta)\tilde{\theta} \tag{3.8}$$

Using equation 3.2 one gets:

$$MJ^{-1}(\eta)[\ddot{\tilde{\eta}} - K_d\dot{\tilde{\eta}} - K_p\tilde{\eta}] = \Phi(a^b, \nu, \eta)\tilde{\theta} \tag{3.9}$$

The proof of stability for this control system is found in (Fossen, 2002).

3.1.2 Robustness

One of the principal motivations for choosing MRAC to control the vessel is the robustness it exhibits regarding parameter uncertainty. As stated in section 3.1, the controller guarantees tracking, but not parameter convergence. However, the robustness to noise is a different matter altogether. If measures aren't taken, noise can cause parameter drift, which in turn may render the system unstable. Even small disturbances have the potential to make the system unstable (Slotine and Li, 1991). This was confirmed in simulations, where adding noise to the measurements instantly made the system unstable.

In order to counteract the effects of noise, one can add dead-zones to the error signals that are used for parameter estimation. This means that one will ignore small tracking errors, motivated by the fact that a relatively large part of these will be noise.

$$\dot{\hat{\theta}} = \begin{cases} -\Gamma\Phi^T(\ddot{\eta}_r^b, \nu, \eta)J^{-1}(\eta)y, & \text{if } |e| > \Delta \\ 0, & \text{if } |e| < \Delta \end{cases} \tag{3.10}$$

Chapter 4

Simulation

4.1 Implementation

One important aspect is to find a platform on which to implement the system so that real-time requirements are satisfied. Also in (Svendby, 2006) the problem of communication delays was identified.

Some preliminary testing of communication was performed in C on a Linux platform. However, as Matlab/Simulink provides great opportunities for matrix operations, and the Real-Time Workshop toolbox addresses the real-time issues, this platform was chosen for the implementation of the control system.

The control system was initially developed as a script in Matlab, and later adjusted for use with the Matlab Embedded Function block in Simulink. The resulting Simulink model was then compiled/built with Real-Time Windows Target so that it could run in external mode. In external mode the compiled model is run in the Matlab Real-Time Kernel.

4.1.1 Guidance

To produce the desired trajectories that the vessel should follow, the following equations are used.

A reference model is used to produce the desired heading, ψ_d, and yaw rate, $r_d = \dot{\psi}_d$. It is given by:

$$\ddot{\psi}_d + 2\delta\omega\dot{\psi}_d + \omega^2\psi_d = \omega^2\psi_r \tag{4.1}$$

where δ is the relative damping ratio and ω is the natural frequency. ψ_r is the

reference heading given by:

$$\psi_r = \arctan \frac{y_k - y}{x_k - x} \tag{4.2}$$

(x_k, y_k) are the coordinates of the current waypoint, while (x, y) is the current position of the vessel.

The desired heading is used to determine the desired horizontal path:

$$u_d = U_d \cos(\psi_d) \tag{4.3}$$

$$v_d = U_d \sin(\psi_d) \tag{4.4}$$

U_d is the desired horizontal speed, as defined by:

$$U_d = \sqrt{u_d^2 + v_d^2} \tag{4.5}$$

U_d is determined by:

$$T_d \dot{U}_d + U_d = U_r \tag{4.6}$$

U_r is the reference horizontal speed.

The desired depth of the vessel is governed by the following equation:

$$T_z \dot{z}_d + z_d = z_r \tag{4.7}$$

where the reference depth, z_r, may be the z-coordinate of the current waypoint, or be given by an algorithm that seeks to keep the vessel at a constant distance from the seabed.

The resulting desired velocity vector is given by:

$$\nu_{\mathbf{d}} = \begin{bmatrix} u_d \\ v_d \\ w_d \\ 0 \\ 0 \\ r_d \end{bmatrix}$$

The desired path is given by the set of desired position vectors, η_d, which is found from:

$$\dot{\eta_d} = J(\Theta)\nu_d \tag{4.8}$$

4.2 Simulation

For the simulation presented here, waypoints in three dimensions forming a lawnmower pattern in the horizontal plane were defined.

The vessel starts with zero speed, but the reference horizontal speed, $U_r = 0.3$ m/s. When the vessel enters a vertical cylinder of acceptance about a waypoint the reference horizontal speed is set to zero. It remains equal to zero until the vessel's heading and depth are acceptably close to their reference values, then its value is set back to 0.3 m/s.

The nature of an MRAC system is that its performance improves if its estimated parameters have values close to those of the real vessel parameters. When the initial value of all the parameter estimates is set to zero, the performance of the controller is not optimal, and it demands much more thrust force than the vessel thrusters can supply. Because of these factors, an initialisation run is performed. Then the final values of the parameter estimates are used as initial values for any subsequent simulation run.

The combined error parameter is:

$$\lambda_{\mathbf{0}} = \begin{bmatrix} 10 & 0 & 0 & 0 & 0 & 0 \\ 0 & 10 & 0 & 0 & 0 & 0 \\ 0 & 0 & 10 & 0 & 0 & 0 \\ 0 & 0 & 0 & 10 & 0 & 0 \\ 0 & 0 & 0 & 0 & 10 & 0 \\ 0 & 0 & 0 & 0 & 0 & 10 \end{bmatrix}$$

The controller gains used for the simulation are:

$$\mathbf{K_p} = \begin{bmatrix} 100 & 0 & 0 & 0 & 0 & 0 \\ 0 & 100 & 0 & 0 & 0 & 0 \\ 0 & 0 & 50 & 0 & 0 & 0 \\ 0 & 0 & 0 & 50 & 0 & 0 \\ 0 & 0 & 0 & 0 & 50 & 0 \\ 0 & 0 & 0 & 0 & 0 & 100 \end{bmatrix}$$

$$\mathbf{K_d} = \begin{bmatrix} 20 & 0 & 0 & 0 & 0 & 0 \\ 0 & 20 & 0 & 0 & 0 & 0 \\ 0 & 0 & 20 & 0 & 0 & 0 \\ 0 & 0 & 0 & 1 & 0 & 0 \\ 0 & 0 & 0 & 0 & 1 & 0 \\ 0 & 0 & 0 & 0 & 0 & 10 \end{bmatrix}$$

$$\mathbf{\Gamma} = \begin{bmatrix} 0.5 & 0 & 0 & 0 & 0 & 0 \\ 0 & 0.5 & 0 & 0 & 0 & 0 \\ 0 & 0 & 0.5 & 0 & 0 & 0 \\ 0 & 0 & 0 & 0.5 & 0 & 0 \\ 0 & 0 & 0 & 0 & 0.5 & 0 \\ 0 & 0 & 0 & 0 & 0 & 0.5 \end{bmatrix}$$

However, to obtain the parameter estimate initial values, a different set of controller gains was used:

$$\mathbf{K_p} = \begin{bmatrix} 100 & 0 & 0 & 0 & 0 & 0 \\ 0 & 100 & 0 & 0 & 0 & 0 \\ 0 & 0 & 100 & 0 & 0 & 0 \\ 0 & 0 & 0 & 50 & 0 & 0 \\ 0 & 0 & 0 & 0 & 50 & 0 \\ 0 & 0 & 0 & 0 & 0 & 100 \end{bmatrix}$$

$$\mathbf{K_d} = \begin{bmatrix} 10 & 0 & 0 & 0 & 0 & 0 \\ 0 & 10 & 0 & 0 & 0 & 0 \\ 0 & 0 & 10 & 0 & 0 & 0 \\ 0 & 0 & 0 & 1 & 0 & 0 \\ 0 & 0 & 0 & 0 & 1 & 0 \\ 0 & 0 & 0 & 0 & 0 & 10 \end{bmatrix}$$

$T_z = 50$ seconds, $T_U = 30$ seconds and the threshold from the deadzone (equation 3.10), $\Delta = 0.1$. The radius of the cylinder of acceptance is 1 metre. The position of the end point of the umbilical, $\eta_{cd} = 0$.

Initially,

$$\eta = \begin{bmatrix} 10 \\ 0 \\ 10 \\ 0 \\ 0 \\ 0.7 \end{bmatrix}$$

and $\nu = 0$.

The waypoints are given by the following three vectors:

$$\mathbf{wpt.x} = \begin{bmatrix} 10 & 60 & 58.8 & 8.8 & 7.6 & 57.6 & 56.4 & 6.4 \end{bmatrix}$$

$$\mathbf{wpt.y} = \begin{bmatrix} 10 & 20 & 25.88 & 15.88 & 21.76 & 31.76 & 37.64 & 27.64 \end{bmatrix}$$

$$\mathbf{wpt.z} = \begin{bmatrix} 10 & 15 & 15 & 20 & 20 & 30 & 30 & 20 \end{bmatrix}$$

4.2.1 The Vessel Model

In this simulation, the parameters of equations 2.2 and 2.3 are:

$$\mathbf{M} = \begin{bmatrix} 405 & 0 & 0 & 0 & 121.5 & 0 \\ 0 & 405 & 0 & -121.5 & 0 & 0 \\ 0 & 0 & 405 & 0 & 0 & 0 \\ 0 & -121.5 & 0 & 98.21 & 0 & 0 \\ 121.5 & 0 & 0 & 0 & 164.14 & 0 \\ 0 & 0 & 0 & 0 & 0 & 129.22 \end{bmatrix}$$

$$\mathbf{D_l} = \begin{bmatrix} 300 & 0 & 0 & 0 & 0 & 0 \\ 0 & 300 & 0 & 0 & 0 & 0 \\ 0 & 0 & 300 & 0 & 0 & 0 \\ 0 & 0 & 0 & 100 & 0 & 0 \\ 0 & 0 & 0 & 0 & 100 & 0 \\ 0 & 0 & 0 & 0 & 0 & 100 \end{bmatrix}$$

$$\mathbf{D_q} = \begin{bmatrix} 280.5 & 0 & 0 & 0 & 0 & 0 \\ 0 & 563.5 & 0 & 0 & 0 & 0 \\ 0 & 0 & 578.2 & 0 & 0 & 0 \\ 0 & 0 & 0 & 100 & 0 & 0 \\ 0 & 0 & 0 & 0 & 100 & 0 \\ 0 & 0 & 0 & 0 & 0 & 100 \end{bmatrix}$$

$$\mathbf{K_{cd}} = \begin{bmatrix} -10 & 0 & 0 & 0 & 0 & 0 \\ 0 & -10 & 0 & 0 & 0 & 0 \\ 0 & 0 & -10 & 0 & 0 & 0 \\ 0 & 0 & 0 & 0 & 0 & 0 \\ 0 & 0 & 0 & 0 & 0 & 0 \\ 0 & 0 & 0 & 0 & 0 & 0 \end{bmatrix}$$

$$\mathbf{w} = \begin{bmatrix} 100 \\ -50 \\ 0 \\ 0 \\ 0 \\ 0 \end{bmatrix}$$

The parameters used to find $g(\eta)$ are $W = 405$ N and $B = 400$ N.

$$\mathbf{r_g} = \begin{bmatrix} 0 \\ 0 \\ 0.3 \end{bmatrix}$$

and $r_b = 0$.

The M matrix is approximated using the mass and shape of the ROV Minerva. The D_q matrix is found using the projected area in the case of the first three DOF. The last three are chosen to be reasonable values in relation to the first three DOF. All off-diagonal elements are set to zero, as these have little impact on the model.

The D_l matrix is chosen in a similar way to D_q, but here all values are chosen and none calculated.

4.2.2 Simulation Results

In this section the most relevant plots from the simulation are presented. The reader is referred to Appendix A for the remaining plots.

In figure 4.1 the lawnmower pattern that the vessel travels is displayed.

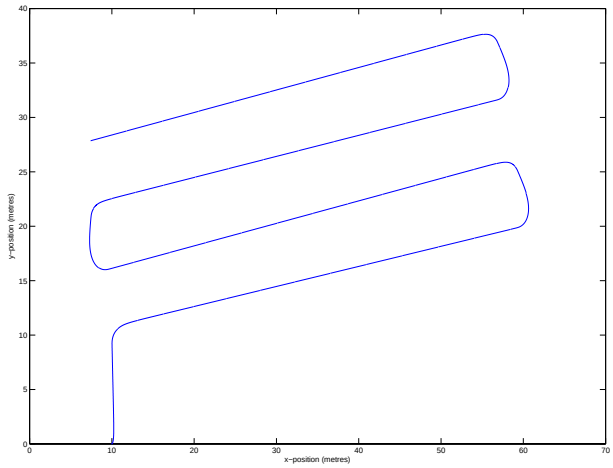

Figure 4.1: The path travelled in the xy-plane

η as a function of time is shown in figure 4.2 . One can verify that the vessel reaches the desired waypoints definded in surge, sway and heave. In roll and pitch the deviation from zero is not very large.

The error in position and orientation is presented in figure 4.3. The error is very small, but increases when the vessel reaches a new waypoint.

Reduced Damping in Yaw

The experiments carried out suggest that the damping in yaw is very small, and that this causes problems controlling the heading. To investigate this further, the yaw element on the diagonal of the damping matrices is reduced from 100 to 1 and the simulation is performed again. The error in position and orientation, $\tilde{\eta}$, from this alternate simulation is shown in figure 4.4.

Comparing figures 4.3 and 4.4, it is evident that the vessel with the most damping experiences a greater error when switching waypoints. Also, its response to this error is slower.

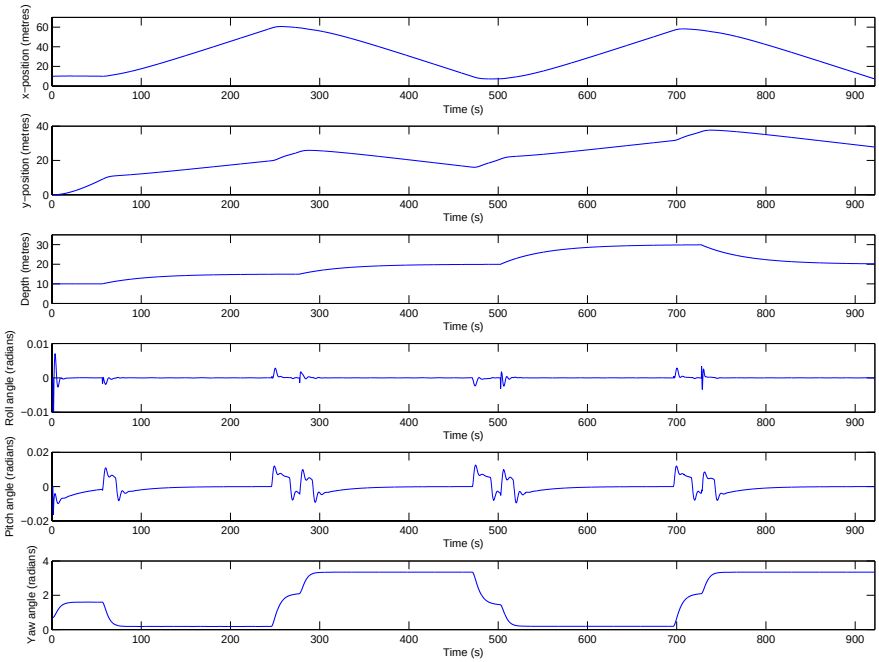

Figure 4.2: η as a function of time

Without Lateral Thruster

If the lateral thruster does not work, but the control allocation remains the same (section 5.1.2), the control system does not work at all. The vessel is moving about, but is totally out of control.

Changing the control allocation to account for the lack of the lateral thruster did not resolve the problem. As it is an underactuated problem to control the vessel in four DOF with three thrusters, the sway mode had to be removed from the commanded force vector. It is clear that in order to make the vessel work without the lateral thruster a more elaborate analysis of the underactuated problem is necessary.

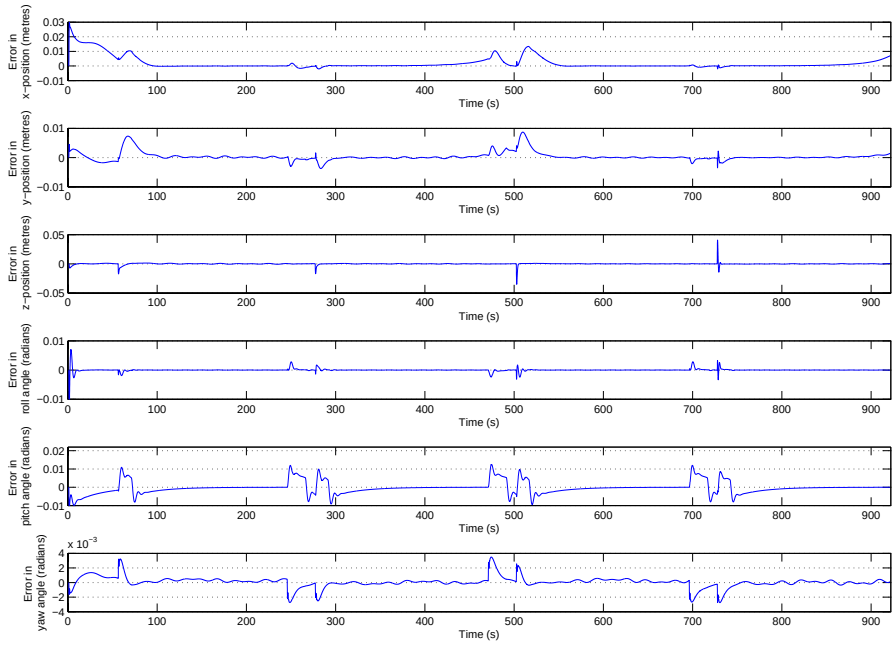

Figure 4.3: $\tilde{\eta}$ as a function of time

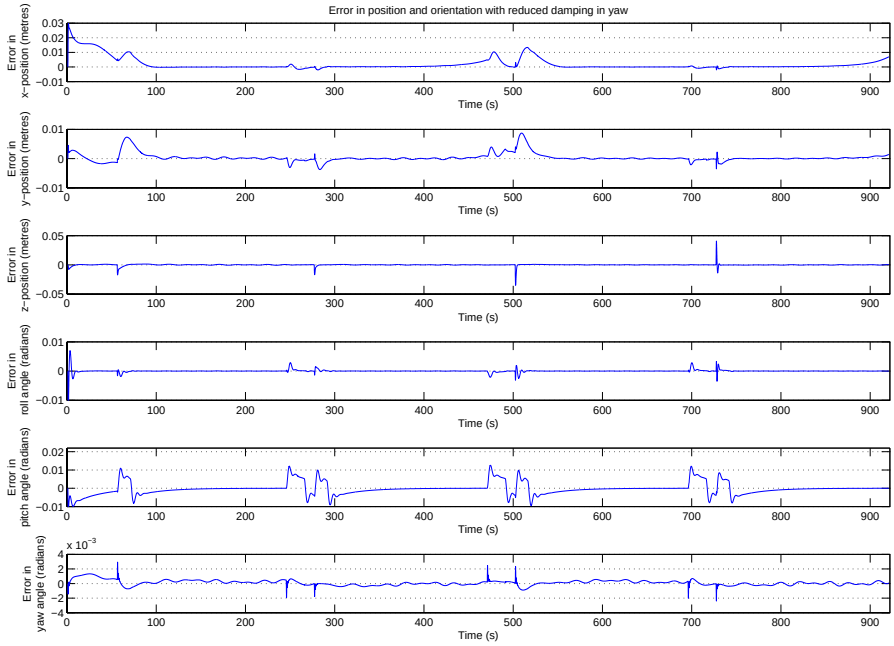

Figure 4.4: $\tilde{\eta}$ as a function of time with reduced damping in yaw

Chapter 5

Practical Experiments

The controller was tested with the ROV Minerva in experiments performed from the R/V Gunnerus on the 14th and 15th of May 2007.

5.1 Implementation

5.1.1 Communication and Real-Time Execution

A vital part of the control system, when used for practical experiments, is the communication with the vessel.

The commanded force to the thrusters is communicated to the ROV Minverva through the umbilical, instead of using the control console that normally steers the vessel. The details of the data telegram sent can not be disclosed by agreement with Sperre AS.

The measurements of the position and orientation of R/V Gunnerus are obtained from the GPS onboard (Seatex DPS116). The position of ROV Minerva relative to R/V Gunnerus are obtained from a HiPAP SSBL system, and the surge velocity is given by a RDI Navigator 600kHz DVL. These measurements are processed by the navigation program Navipac, and transmitted as strings of characters on a serial line, using the RS-232 protocol, to the control computer.

The measurements of the depth, heading and yaw rate are obtained from instruments on the ROV, and are transmitted directly to the control computer using the RS-232 protocol.

Using the built-in functions for serial communication that Matlab offers is not a good option as they are too slow. Using them would introduce time delays

in the control loop. This is unacceptable for applications with fast dynamics, such as the one in question. It was shown in (Svendby, 2006) that the time delay renders the controller useless.

Aiming to address the real-time issues, Real-Time Workshop was going to be used. Utilising the Real-Time Windows Target, the Simulink implementation of the controller was compiled to be run in external mode. In order to read to and write from the serial ports, S-functions was written in C and included in the Simulink model. However, the Real-Time Windows Target imposes severe limitations on the number of library C functions that can be used in S-functions in the model. Because of this, it was not possible to read the measurement data from the serial port with the necessary reliability.

After exhaustively attempting to make the communication work with Real-Time Workshop, it was deemed necessary to abandon it. The solution was to use a set of RS-232 blocks and a Real-Time block from (Daga, 2006). They are also available at Mathworks' Matlab Central. The Real-Time block makes the Simulink model run in real-time without compiling.

5.1.2 Control Allocation

The controller calculates a force and moment vector, τ, in six DOF, that should be applied to the vessel. To do this, the forces and moments in τ must be translated into force output by each of the five thrusters, given by the vector u. The relation between τ and u is given by:

$$\tau = T(\alpha)u \tag{5.1}$$

where $T(\alpha)$ is the actuator configuration matrix and α is a vector of angles of the thrusters. u is a column vector composed of:

- u_1 - force from the lateral thruster
- u_2 - force from each of the two vertical thrusters
- u_3 - force from the port thruster
- u_4 - force from the starboard thruster.

For the ROV Minerva, the angles of the thrusters are fixed. The angles of the port and starboard thrusters are $-10°$ and $10°$ respectively.

Using figures 5.1 and 5.2, and assuming the centre of gravity in the xy-plane to be in $(\frac{\text{total length}}{2}, \frac{\text{total breadth}}{2})$ and the centre of gravity on the z-axis

to be in the lower part of the ROV one can verify that, given the relation in equation 5.1:

$$\mathbf{T}(\alpha) = \begin{bmatrix} 0 & 0 & \cos(-10^\circ) & \cos(10^\circ) \\ 1 & 0 & \sin(-10^\circ) & \sin(10^\circ) \\ 0 & 2 & 0 & 0 \\ -l_{z1} & 0 & -l_{z4}\sin(-10^\circ) & -l_{z5}\sin(10^\circ) \\ 0 & -l_{x2} & l_{z4}\cos(-10^\circ) & l_{z5}\cos(10^\circ) \\ l_{x1} & 0 & l_{x4}\sin(-10^\circ) - l_{y4}\cos(-10^\circ) & l_{x5}\sin(10^\circ) - l_{y5}\cos(10^\circ) \end{bmatrix},$$

where

$$\begin{aligned} l_{x1} &= 0.163\text{m} \\ l_{z1} &= -0.03\text{m} \\ l_{x4} &= -0.570\text{m} \\ l_{y4} &= -0.30\text{m} \\ l_{z4} &= 0.42\text{m} \\ l_{x5} &= -0.570\text{m} \\ l_{y5} &= 0.30\text{m} \\ l_{z5} &= 0.42\text{m} \end{aligned}$$

These values are approximated, since the actual location of the centre of gravity is unknown, and can move.

(Sørensen, 2005) presents a procedure for finding $T(\alpha)$.

The number of actuators is less than the number of degrees of freedom, hence the ROV is underactuated and the $T(\alpha)$ is not invertible. It is, however, possible to find a pseudo-inverse, $T^\dagger$. Unfortunately, in the case of ROV Minerva

$$TT^\dagger \neq I \tag{5.2}$$

It is the roll and pitch modes that are difficult to control, as the control forces in these modes are lost in the translation $TT^\dagger$. This motivates a reduction in the number of DOF that will be controlled. If one ignores the roll and pitch elements in τ, one can translate this vector into individual thruster force using:

$$\mathbf{T_4}(\alpha) = \begin{bmatrix} 0 & 0 & \cos(-10^\circ) & \cos(10^\circ) \\ 1 & 0 & \sin(-10^\circ) & \sin(10^\circ) \\ 0 & 2 & 0 & 0 \\ l_{x1} & 0 & l_{x4}\sin(-10^\circ) - l_{y4}\cos(-10^\circ) & l_{x5}\sin(10^\circ) - l_{y5}\cos(10^\circ) \end{bmatrix}$$

This reduction can be justified by assuming that the roll and pitch modes are stable; they will always return to zero if perturbated.

5.1.3 Mapping between Thrust Force and Rotational Speed

After distributing the control forces on the various thrusters, the forces need to be transformed into rotational speed for each thruster. The relation is given by

$$u = K_t \rho D^4 |n| n \tag{5.3}$$

where:

- u - force from thruster
- K_t - thrust coefficient for thruster
- ρ - density of water
- n - revolutions per second
- D - propeller diameter.

ρ and D are known, but the thrust coefficient, K_t, presents significant problems. K_t depends on the advance number, J, which in turn depends on the water velocity into the propeller, V_a, and revolutions per second, n.

Measurements of V_a were not available for the experiment, hence finding J was impossible. According to (Smogeli and Sørensen, 2006), one often assumes $J = 0$, and uses the constant K_{t0}. The expressions for K_t supplied by (Ludvigsen and Ødegaard, 2006) cannot be linearised in this manner, as some of them would yield negative values for K_{t0}. K_t must always be strictly positive.

Instead, inserting maximum rotational speed of the thrusters, and maximum force shown by the ROV in all directions into equation 5.4 yields the unknown parameter h in the generalisation of equation 5.3:

$$u = h |n| n \tag{5.4}$$

The maximum force is found in bollard pull experiments referred in (Ludvigsen and Ødegaard, 2006).

5.1.4 Measurements

As well as position and orientation of the mother ship, measurements of six DOF were available for the ROV. These were:

- x - position North
- y - position East
- z - depth
- ψ - heading
- v - forward velocity
- r - yaw rate

5.1.5 Settings

The estimation of the cable drag was removed in the experiment because its contribution to the commanded thrust force was enormous. It caused all the thrusters to reach their saturation values. This could be caused by too high initial values of the estimated parameters or too high gain values in the adaptation law for these parameters.

The initial values of the estimated parameters are the same as for the simulation.

The model runs at 10 Hz, the commanded thrust is sent to the thrusters at a rate of 5 Hz and the measurements are received at a rate of 2 Hz.

When the experiment was carried out, the following gain matrices were used:

$$\mathbf{K_p} = \begin{bmatrix} 1 & 0 & 0 & 0 & 0 & 0 \\ 0 & 1 & 0 & 0 & 0 & 0 \\ 0 & 0 & 4 & 0 & 0 & 0 \\ 0 & 0 & 0 & 0 & 0 & 0 \\ 0 & 0 & 0 & 0 & 0 & 0 \\ 0 & 0 & 0 & 0 & 0 & 0.5 \end{bmatrix}$$

$$\mathbf{K_d} = \begin{bmatrix} 0.3 & 0 & 0 & 0 & 0 & 0 \\ 0 & 0.3 & 0 & 0 & 0 & 0 \\ 0 & 0 & 0 & 0 & 0 & 0 \\ 0 & 0 & 0 & 0 & 0 & 0 \\ 0 & 0 & 0 & 0 & 0 & 0 \\ 0 & 0 & 0 & 0 & 0 & 0.5 \end{bmatrix}$$

$$\lambda_{\mathbf{0}} = \begin{bmatrix} 0.005 & 0 & 0 & 0 & 0 & 0 \\ 0 & 0.005 & 0 & 0 & 0 & 0 \\ 0 & 0 & 0.005 & 0 & 0 & 0 \\ 0 & 0 & 0 & 0 & 0 & 0 \\ 0 & 0 & 0 & 0 & 0 & 0 \\ 0 & 0 & 0 & 0 & 0 & 0.005 \end{bmatrix}$$

$$\mathbf{\Gamma} = \begin{bmatrix} 0.5 & 0 & 0 & 0 & 0 & 0 \\ 0 & 0.5 & 0 & 0 & 0 & 0 \\ 0 & 0 & 0.5 & 0 & 0 & 0 \\ 0 & 0 & 0 & 0.5 & 0 & 0 \\ 0 & 0 & 0 & 0 & 0.5 & 0 \\ 0 & 0 & 0 & 0 & 0 & 0.5 \end{bmatrix}$$

$T_z = 50$ seconds, $T_U = 30$ seconds and the threshold from the deadzone (equation 3.10), $\Delta = 0.1$. The radius of the cylinder of acceptance is 3 metres.

The waypoints are given by the following three vectors:

$$\mathbf{wpt.x} = \begin{bmatrix} 7035178 & 7035185 & 7035177 & 7035168 \end{bmatrix}$$

$$\mathbf{wpt.y} = \begin{bmatrix} 567985 & 567931 & 567930 & 567984 \end{bmatrix}$$

$$\mathbf{wpt.z} = \begin{bmatrix} 65 & 65 & 65 & 70 \end{bmatrix}$$

The values used in the mapping between thrust force and rotational speed were:

starboard/port thrusters, $u \geq 0$	66
starboard/port thrusters, $u < 0$	98
lateral	73
vertical	103

After the experiment was performed, an error in the mapping code was discovered. The lateral thruster was assigned the same mapping as the starboard and port thrusters, meaning that a commanded thrust force would produce different force values depending on the sign of the commanded force.

5.2 Results

In this section the most relevant plots from the practical experiment are presented. The reader is referred to Appendix B for the remaining plots. There are a lot fewer plots compared to the simulation. This is caused by the lack of measurements. Some of the adaptations are driven by variables that are not measured, and hence the parameters remain constant. Plots of these parameters are not included.

The vessel manages to go to the defined waypoints, and to maintain its heading, albeit with some oscillations about the desired heading. The position and heading of the vessel is presented in figure 5.3.

From figure 5.4 one can see the deviation of the actual position and heading from the desired position and heading. It shows that the desired depth is maintained within margins less than 0.5 metres. The error in heading is great for the first 150 seconds, before stabilising with small oscillations about zero. The desired xy-position is maintained within margins of less than 5 metres on each axis. It is worth noticing the occurrence of several drop-outs, that is the measurements become unavailable for a period of time. When the position is maintained exactly the same for a period of time before jumping to a new value, this indicates a drop-out.

If the vessel is stationary, the heading is maintained within margins of 7 degrees (3-4 radians).

Figure 5.5 shows the velocity in surge and the yaw rate of the vessel, both of them exhibiting an oscillatory behaviour.

The thrusters rarely reach their maximum rotational speed of 1450 rounds per minute. Like the velocities, these too are oscillatory. Notably, the vertical thrusters have the smallest oscillations. The depth is also the DOF with the least error. Ideally, the trusters would converge to constant values between waypoints. The rotational speed of the thrusters are presented in figure 5.6.

Figure 5.7 shows the development of the estimated diagonal parameters of the system inertia matrix M. These change as the vessel approaches the first waypoint, and from then stabilise. There are some minor adjustments when changing waypoints.

In figure 5.8 one can see the development of the estimated diagonal parameters of the linear damping matrix D_l. These change steadily throughout the test run. The surge parameter change the most when changing waypoints. The values of these parameters remain insignificantly small. This is also the case with the damping parameters in the simulation (Appendix A).

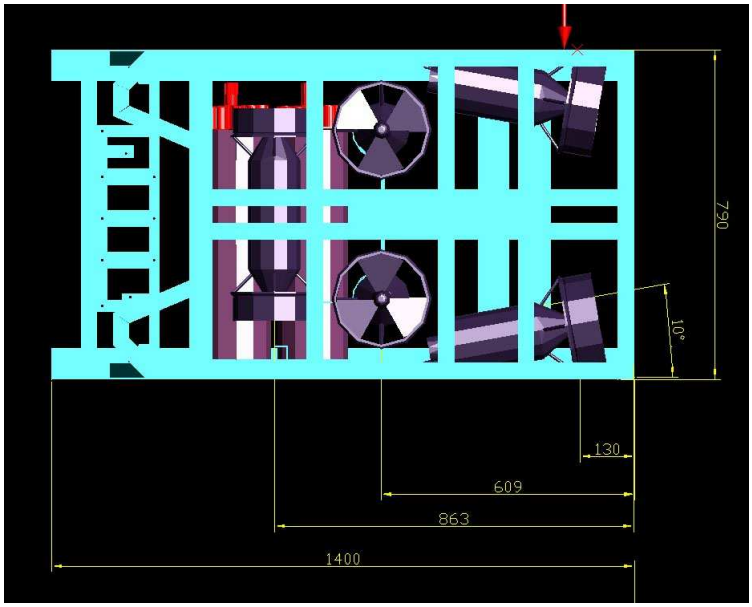

Figure 5.1: Thruster configuration of ROV Minerva, view from top (Courtesy of M. Ludvigsen)

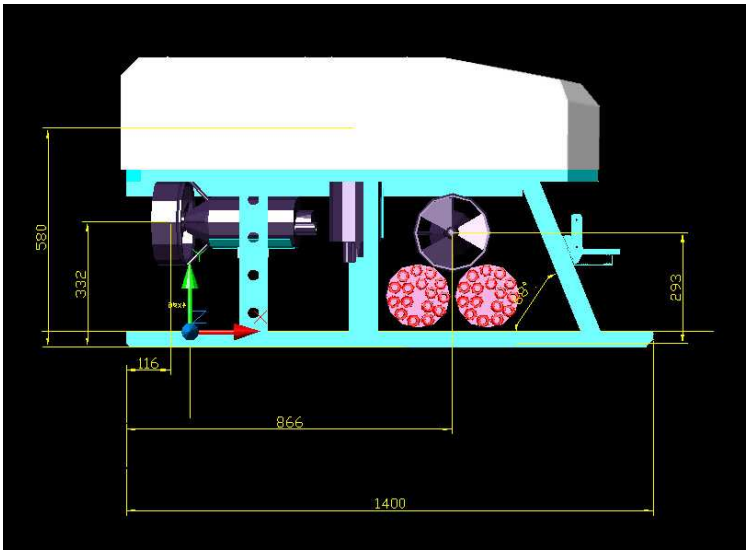

Figure 5.2: Thruster configuration of ROV Minerva, view from side (Courtesy of M. Ludvigsen)

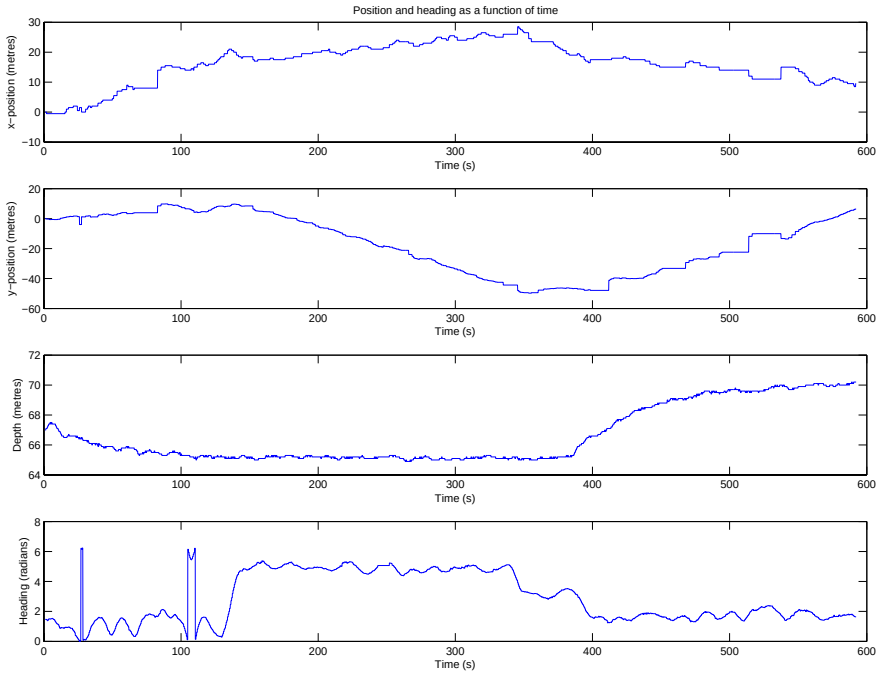

Figure 5.3: η as a function of time

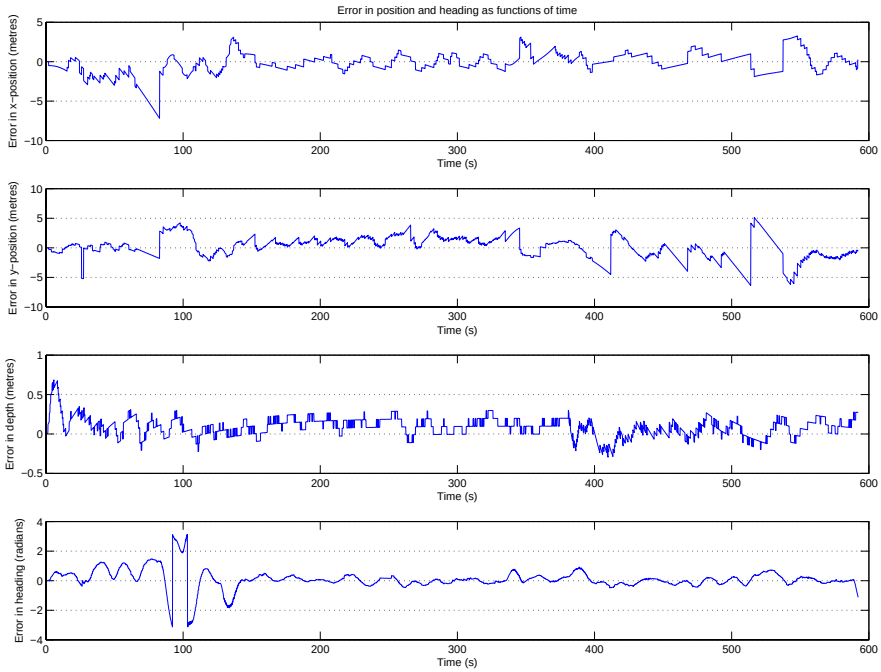

Figure 5.4: $\tilde{\eta}$ as a function of time

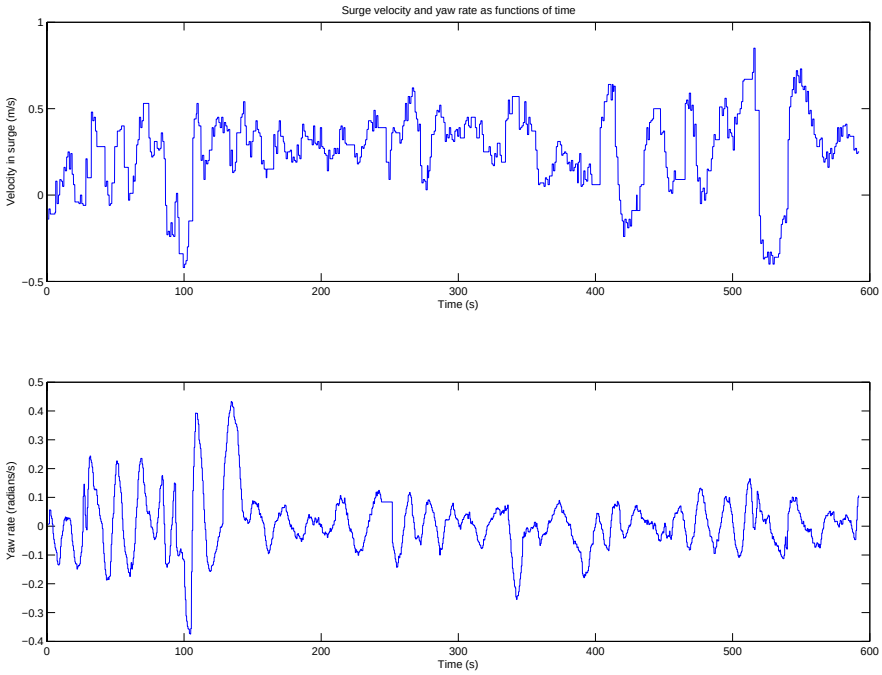

Figure 5.5: ν as a function of time

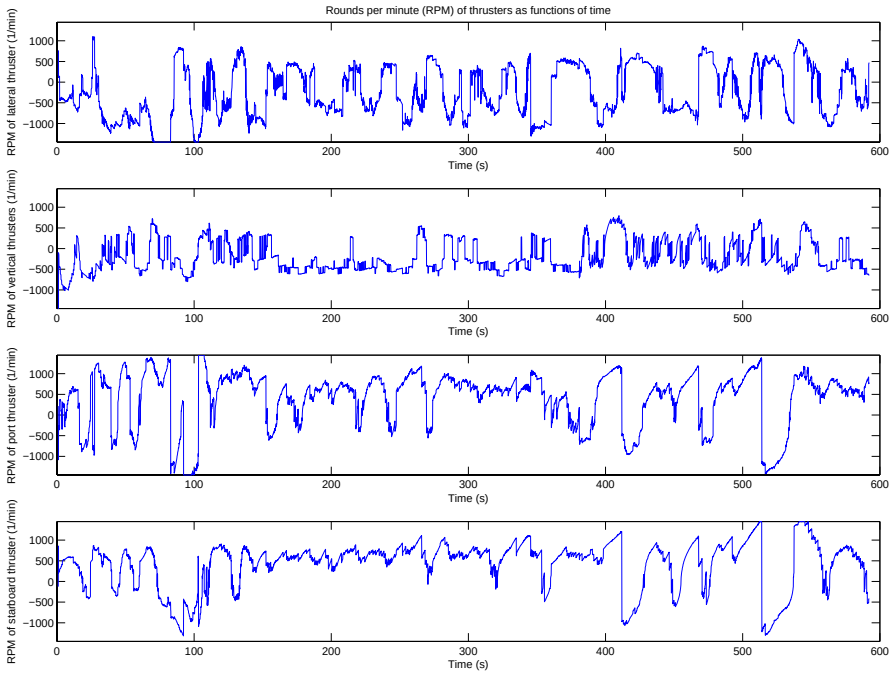

Figure 5.6: RPM of thrusters as a function of time

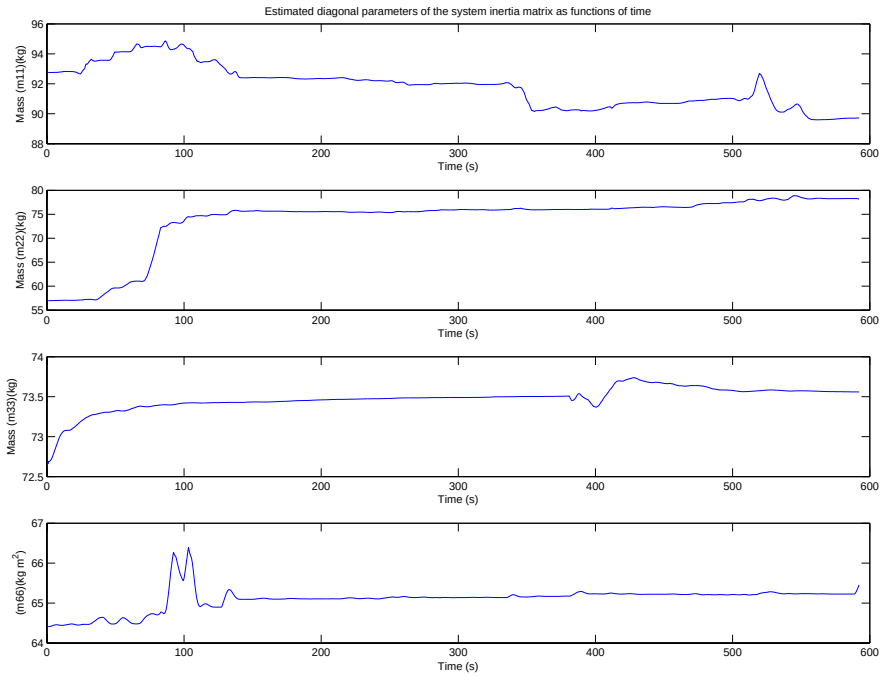

Figure 5.7: Diagonal elements of estimated system inertia matrix as functions of time

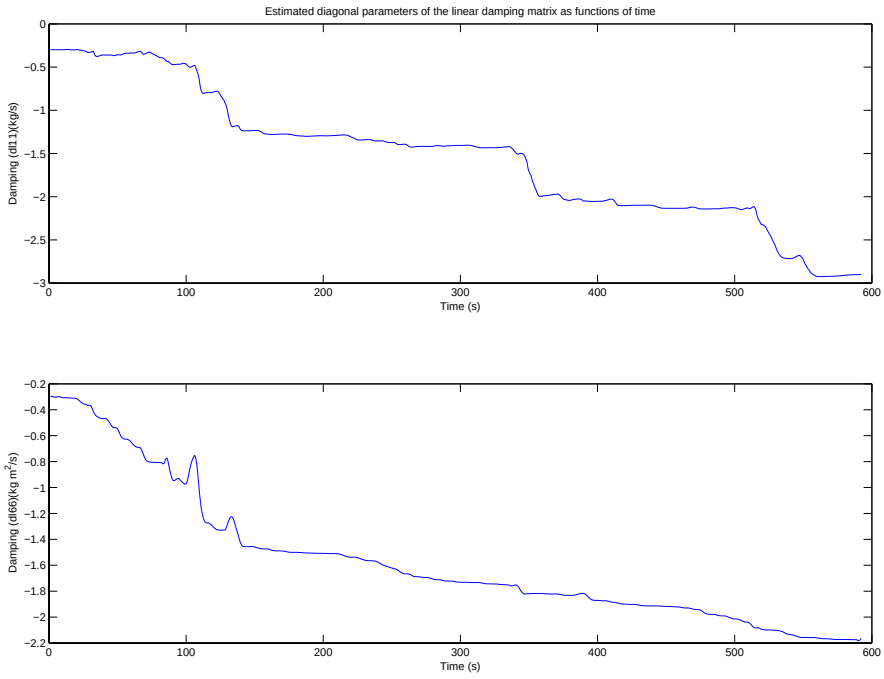

Figure 5.8: Diagonal elements of estimated linear damping matrix as functions of time

Chapter 6

Discussion

The control system shows very good performance in simulations. The deviations from the desired η and ν are minor, although peaking when the vessel reaches a new waypoint and prepares to go to the next. It also exhibits good adaptability to changes in the vessel model.

In the experiments at sea the results are not as good. However, the control system successfully steers the vessel to all the waypoints. The depth control is very good despite the velocity not being measured. The problem seems to be the heading control. Although performing very well when the ROV is stationary, the error is significant when the ROV is moving. This leads to errors in surge and sway, as these two DOF are intimitely connected to the heading.

The most obvious source to this behaviour is the error in the mapping between thrust force and rotational speed for the lateral thruster. This results in that if comparing two instances of commanded thrust force, equal and opposite, would not yield equal and opposite actual forces. This is a likely explanation of the oscillations in the heading. It is surprising that the system did perform as well as it did, considering the graveness of this error.

In the experiment at sea the cable drag was excluded from the controller. Simulating without the cable drag parameters in the control system yielded results inferior to those with the complete controller. The results were still good. In the experiment, before removing the cable drag component, the λ_0 was drastically reduced compared to the value used in simulations. This was because using the larger λ_0 caused the τ to become extremely large. It is possible that removing the cable drag component would eliminate the need for a small λ_0, but this was not confirmed in experiments. A larger λ_0 will increase the response to errors in position and orientation and could have improved the performance of the control system.

The measurements remains a source for improvement. The lack of velocity measurements reduces the performance potential. Including derivative action in the control system would make it more responsive.

It was noted during the experiment that the time constants for velocity and depth were very large. Using smaller values for these time constants will increase the vessel's acceleration in both surge and heave. For bottom tracking, the time constant for depth needs to be much smaller.

Chapter 7

Conclusions

In this project, which is based on the work in (Svendby, 2006), a robust adaptive controller have been developed in order to control the research ROV Minerva. The project aims to control all six degrees of freedom, but only four were achieved; the underactuated nature of the vessel rendered the roll and pitch modes uncontrollable.

The control system was implementented using Matlab and Simulink, running in real-time, but without Real-Time Workshop.

The controller is performing well in simulations. It is also working in the experiment at sea, but the performance is not good enough to be of any practical use. However, the experiment suffered from lack of measurements and a serious error in the mapping between thrust force and rotational speed. Without this error, and with measurements of all states it may be possible to achieve good performance in experiments as well.

Chapter 8

Further Work

A new experiment should be carried out, this time with the correct mapping between thrust force and rotational speed, in order to verify whether the performance is improved enough for the controller to be of practical use.

One should aim to get measurements of all degrees of freedom, alternatively an observer may produce estimates of the states not measured.

The protocol for obtaining the measurements from the instruments should be improved. Ideally, one should custom make programs for this purpose, and compile these before using them in the Simulink model.

Appendix A

Simulation Plots

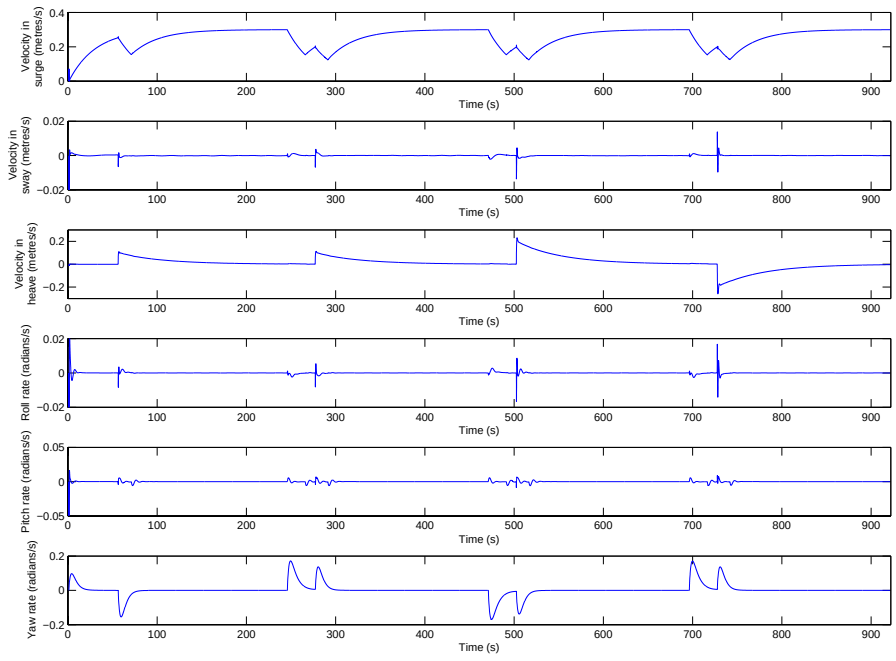

Figure A.1: ν as a function of time

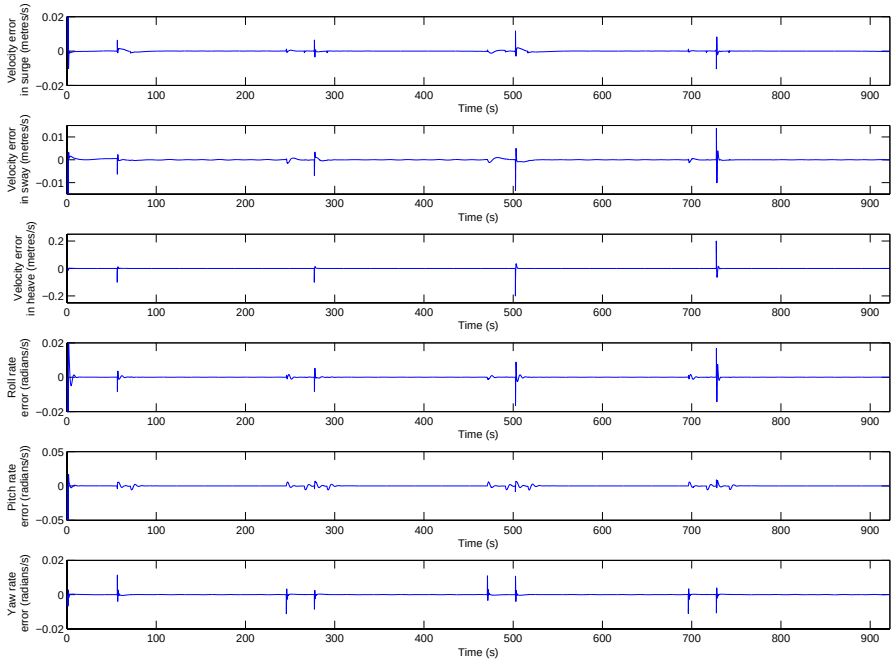

Figure A.2: $\tilde{\nu}$ as a function of time

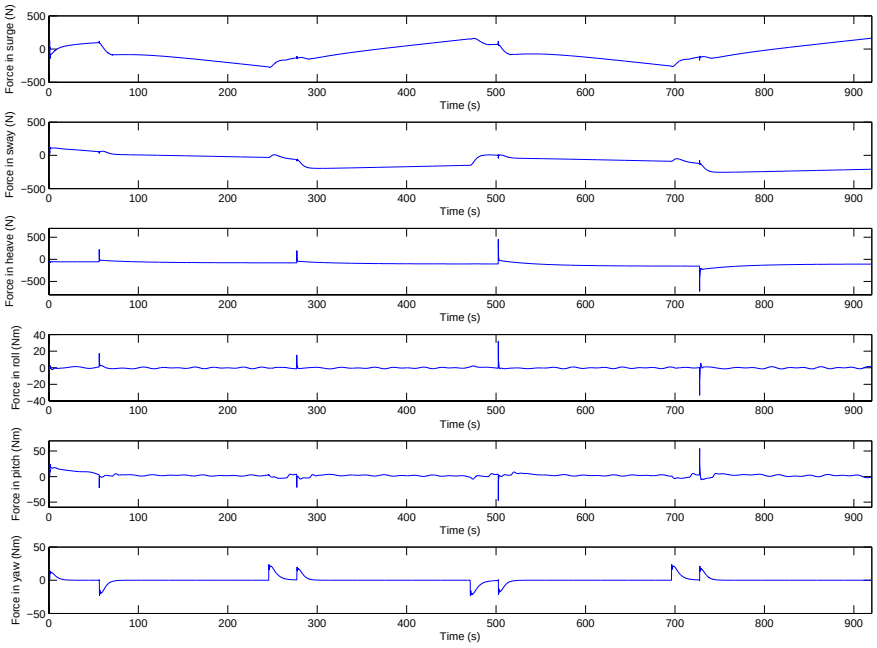

Figure A.3: τ as a function of time

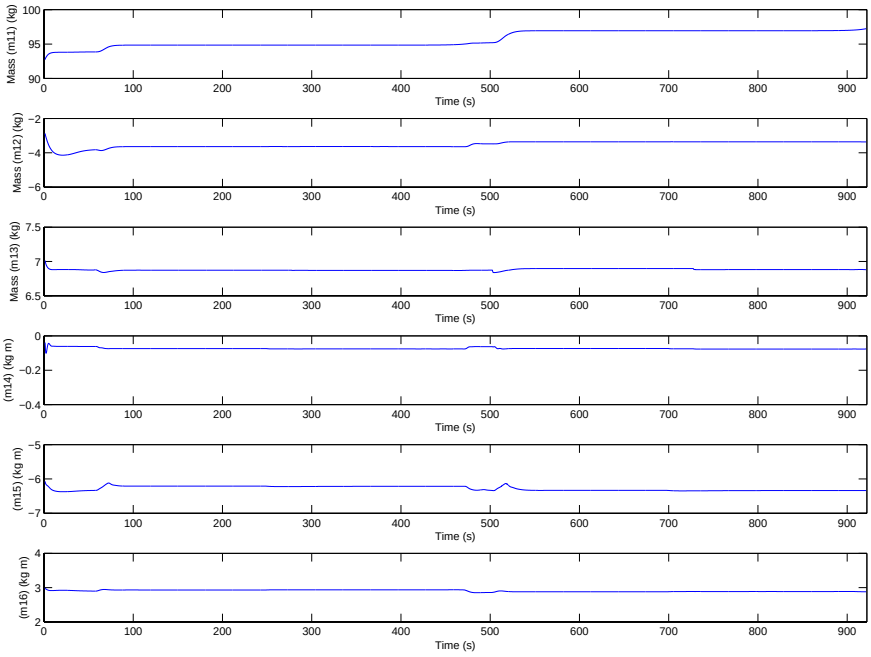

Figure A.4: First row of estimated system inertia matrix

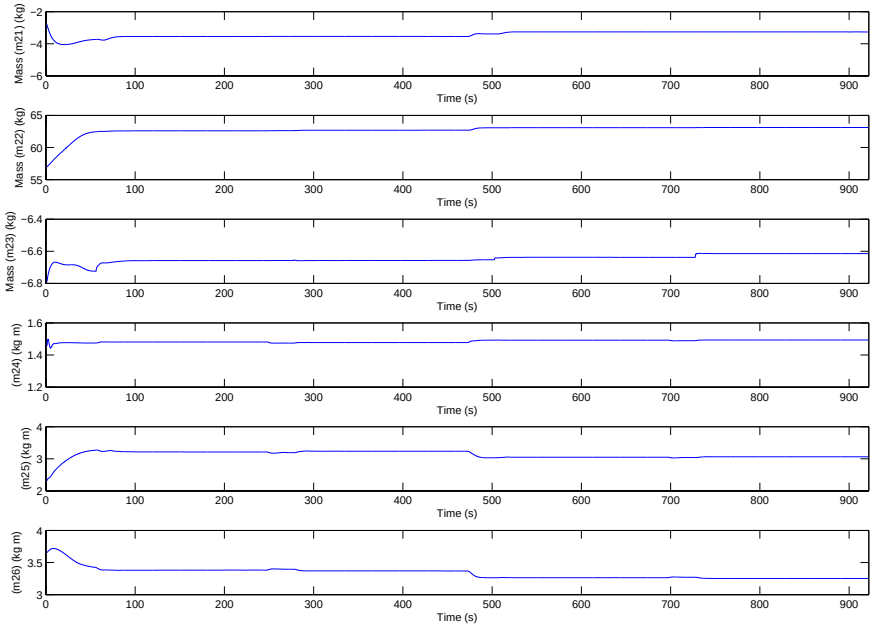

Figure A.5: Second row of estimated system inertia matrix

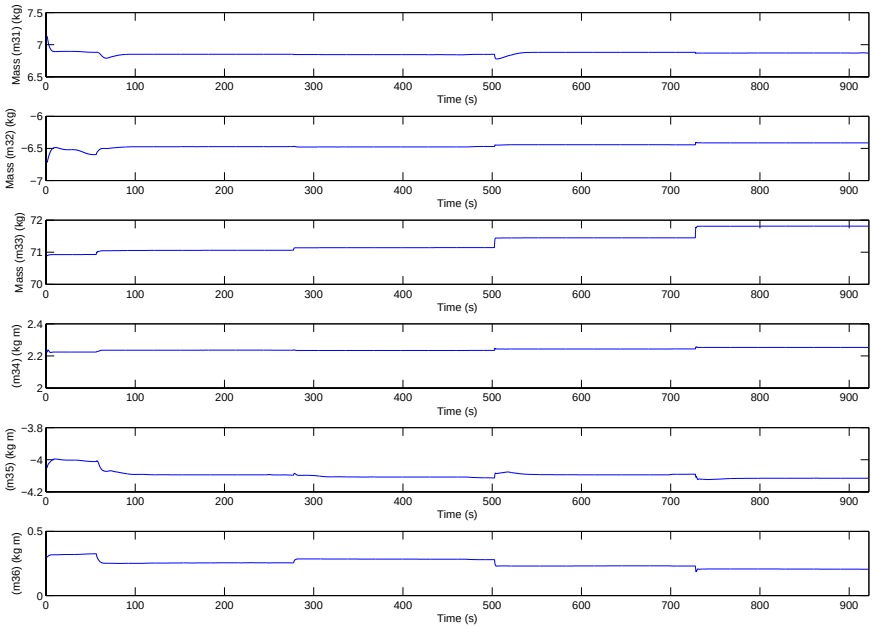

Figure A.6: Third row of estimated system inertia matrix

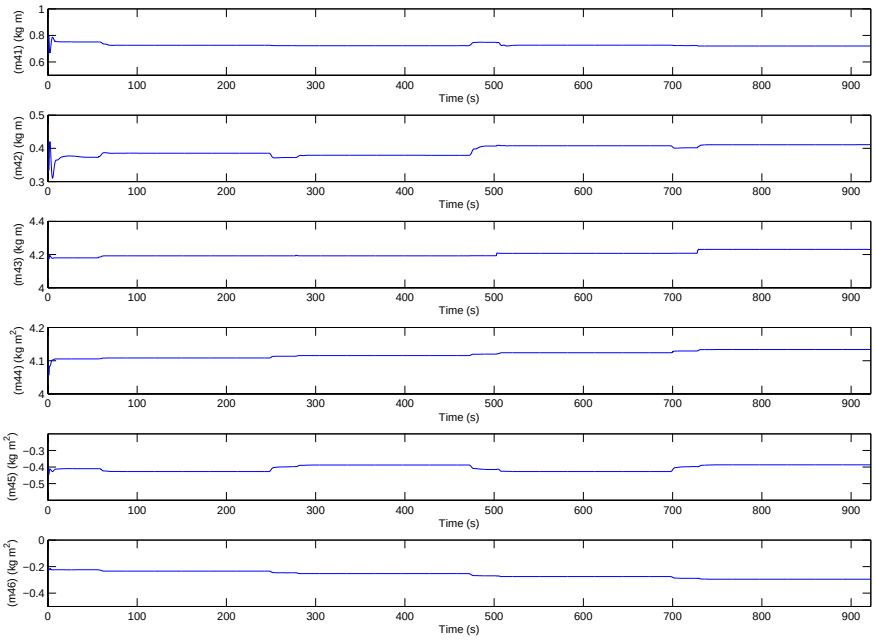

Figure A.7: Fourth row of estimated system inertia matrix

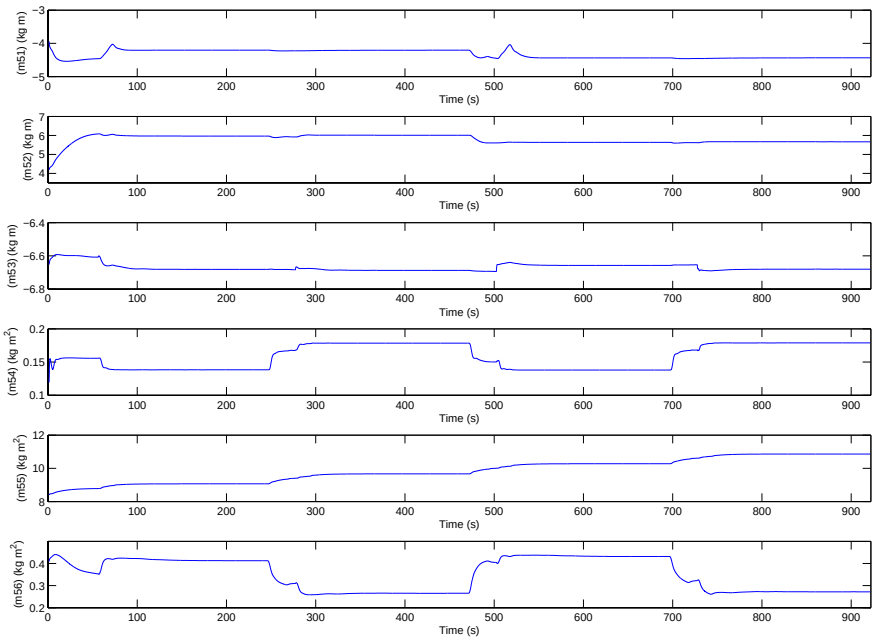

Figure A.8: Fifth row of estimated system inertia matrix

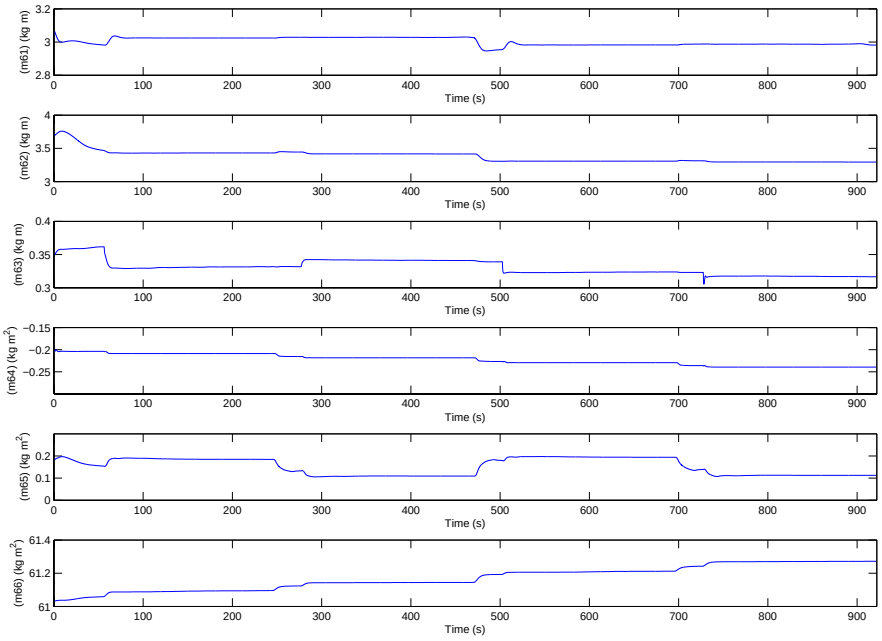

Figure A.9: Sixth row of estimated system inertia matrix

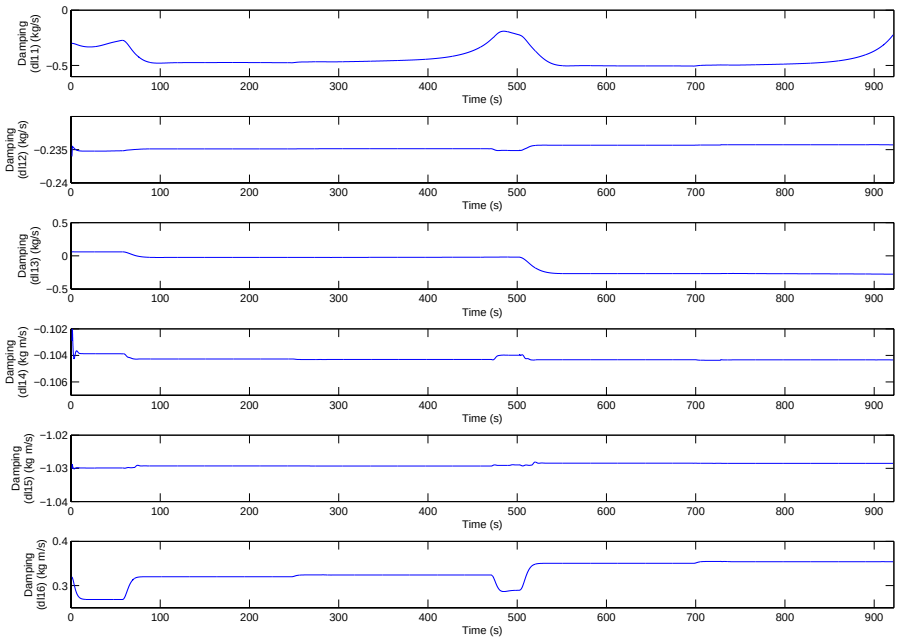

Figure A.10: First row of estimated linear damping matrix

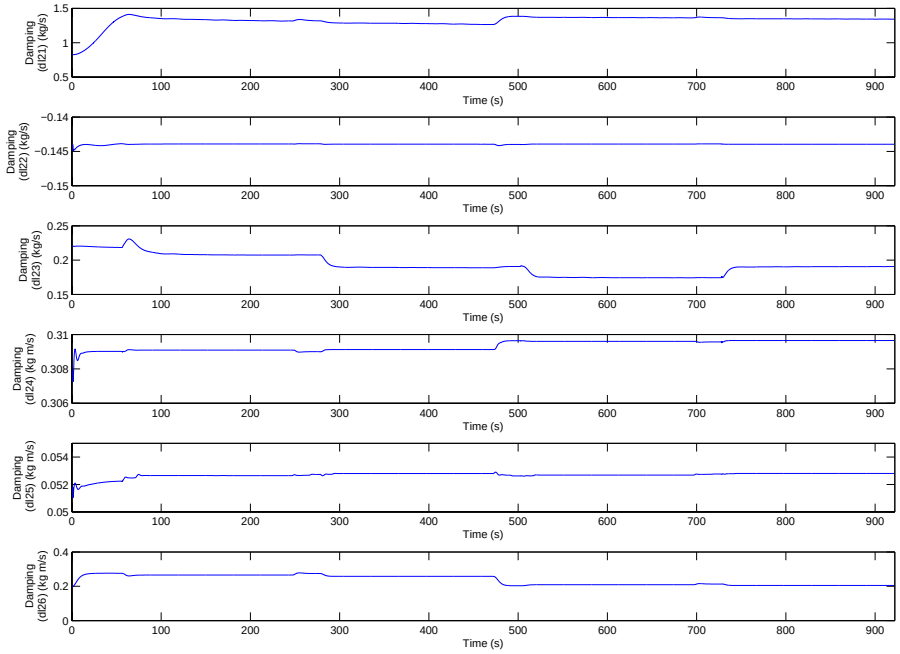

Figure A.11: Second row of estimated linear damping matrix

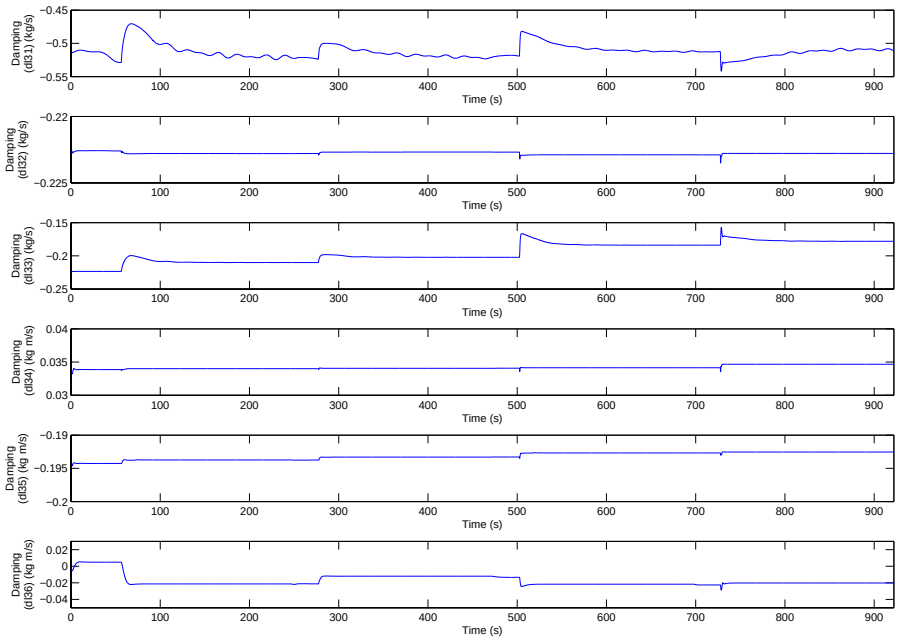

Figure A.12: Third row of estimated linear damping matrix

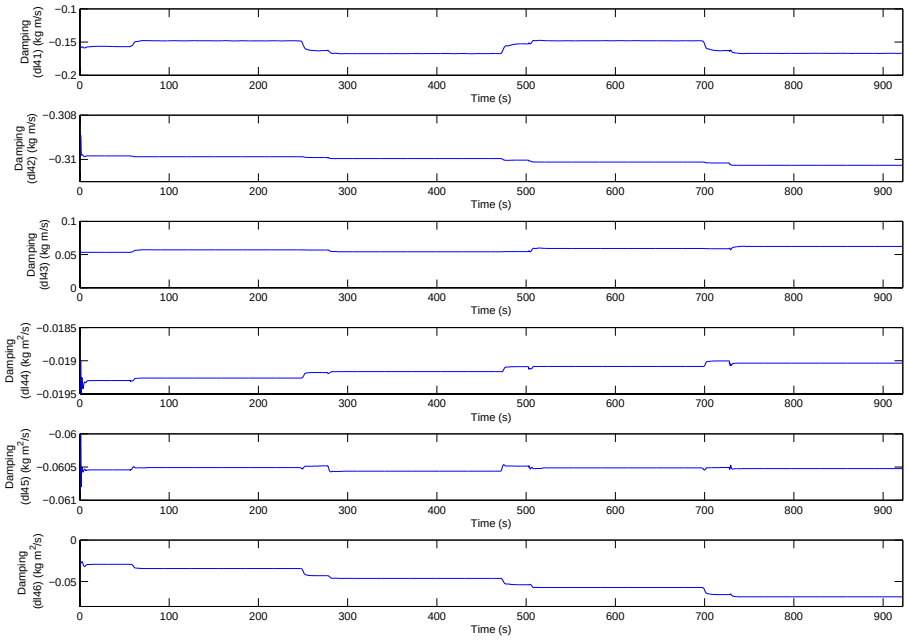

Figure A.13: Fourth row of estimated linear damping matrix

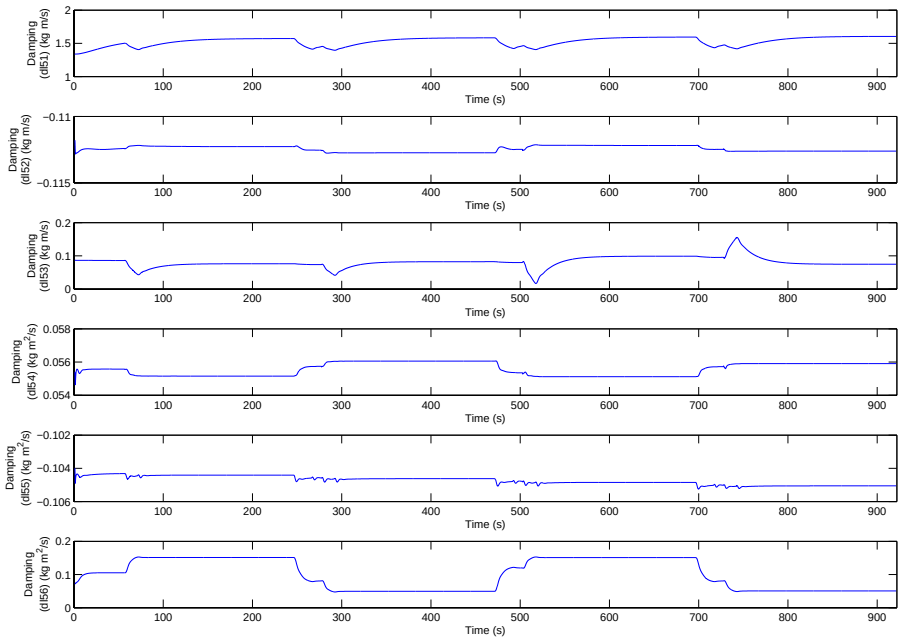

Figure A.14: Fifth row of estimated linear damping matrix

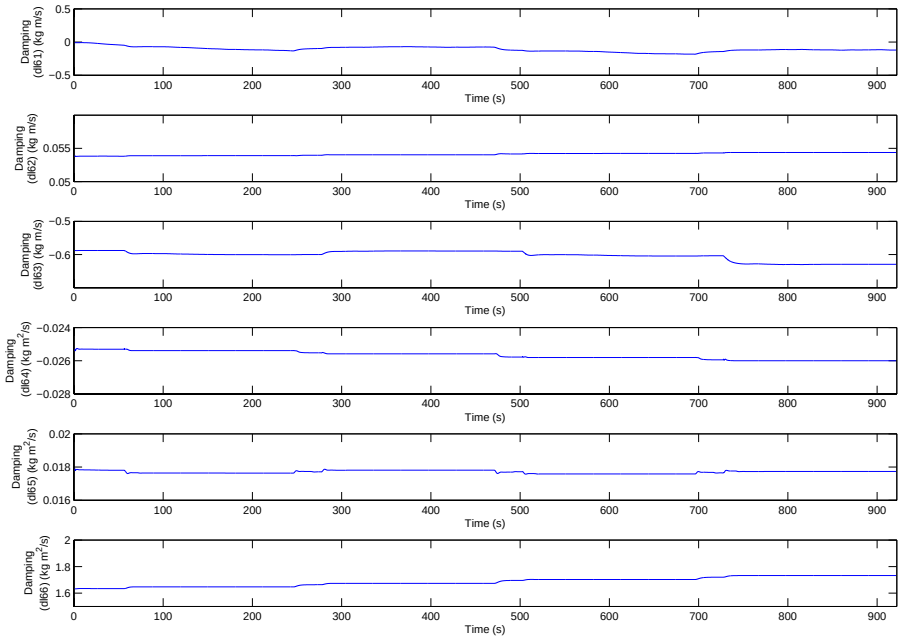

Figure A.15: Sixth row of estimated linear damping matrix

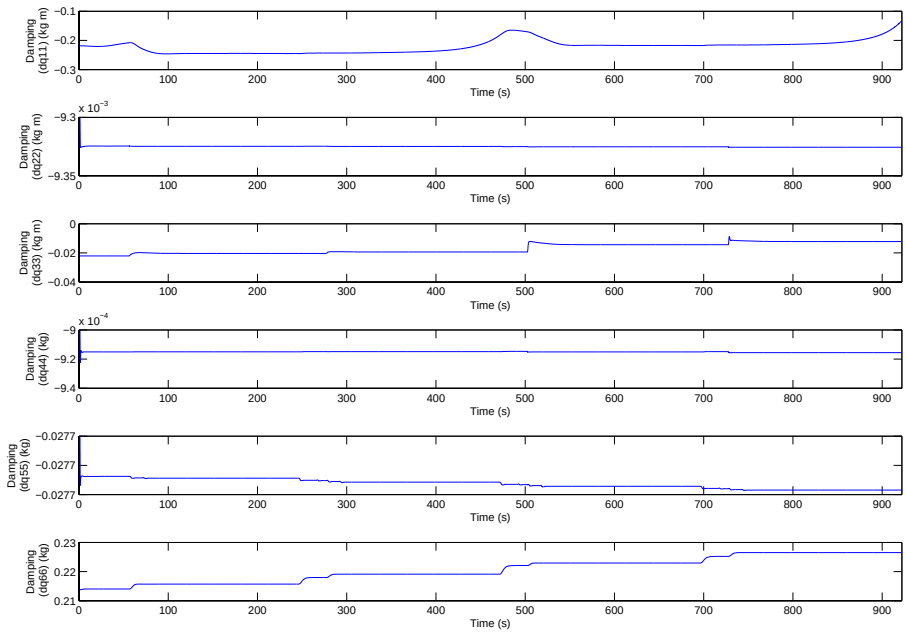

Figure A.16: The estimated quadratic damping matrix

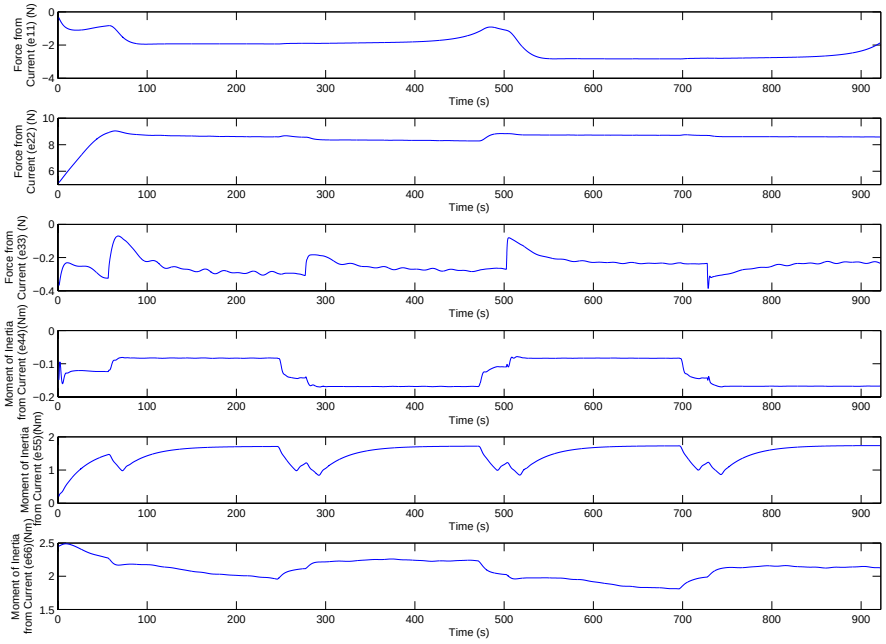

Figure A.17: The estimated environmental disturbance

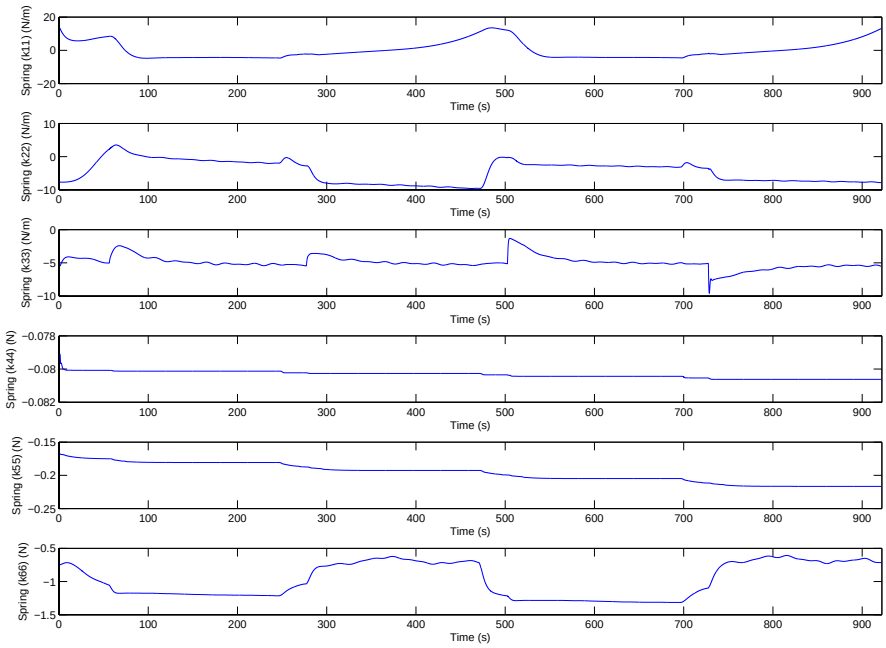

Figure A.18: The estimated spring constant from the cable

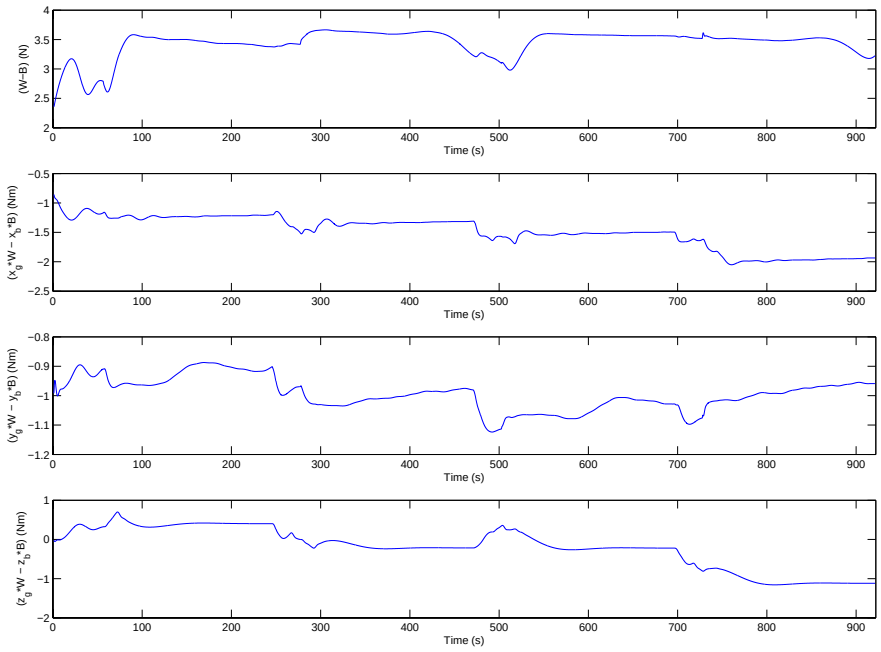

Figure A.19: The estimated gravitational/bouyancy force

Appendix B

Plots from Experiments

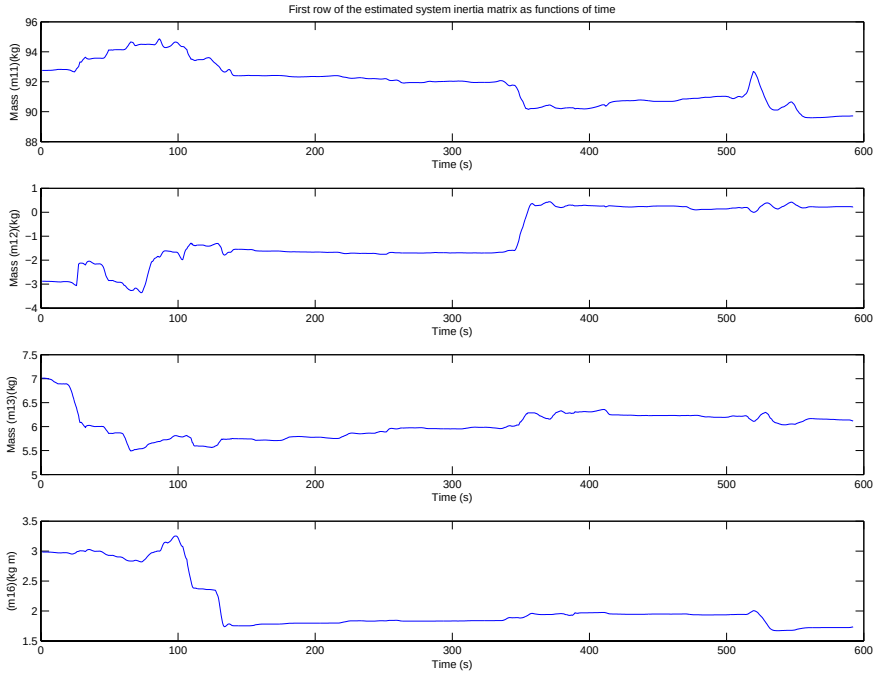

Figure B.1: First row of estimated system inertia matrix as functions of time

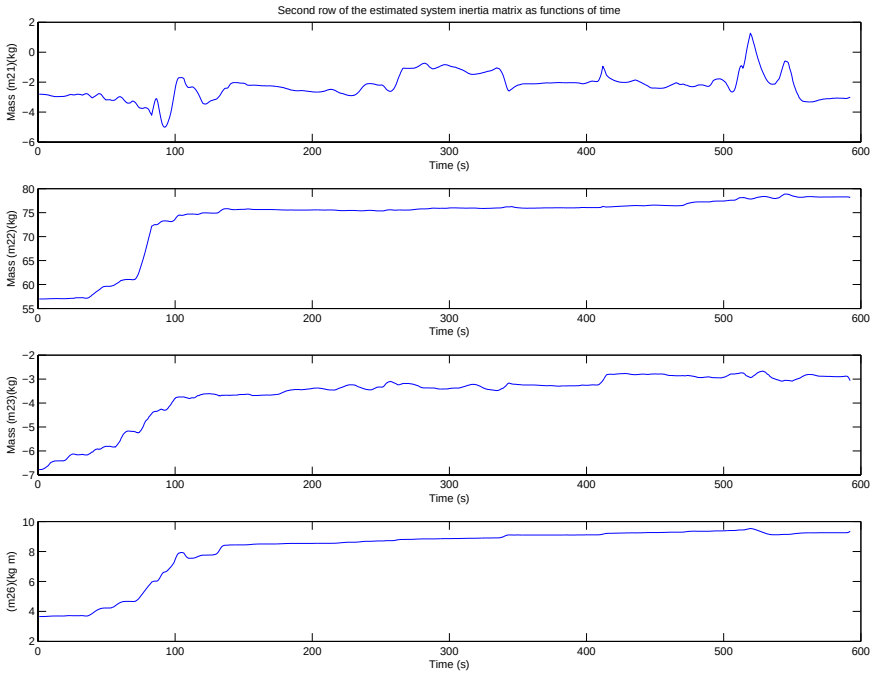

Figure B.2: Second row of estimated system inertia matrix as functions of time

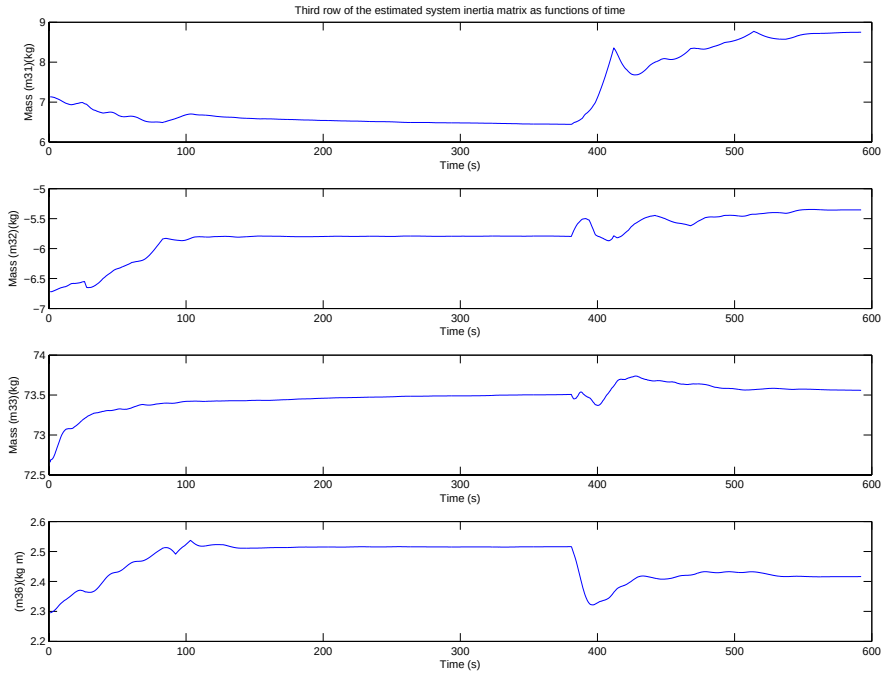

Figure B.3: Third row of estimated system inertia matrix as functions of time

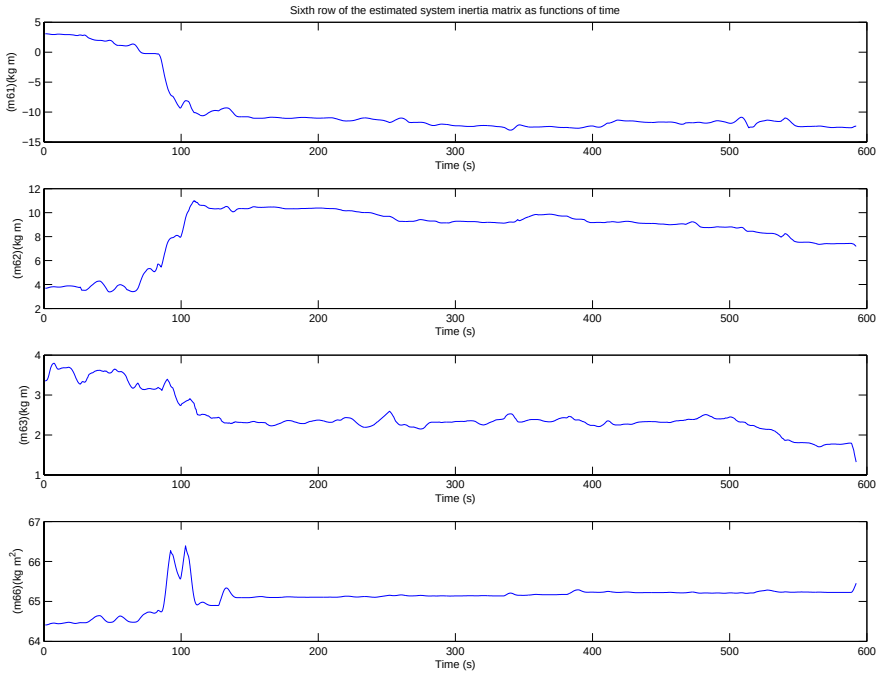

Figure B.4: Sixth row of estimated system inertia matrix as functions of time

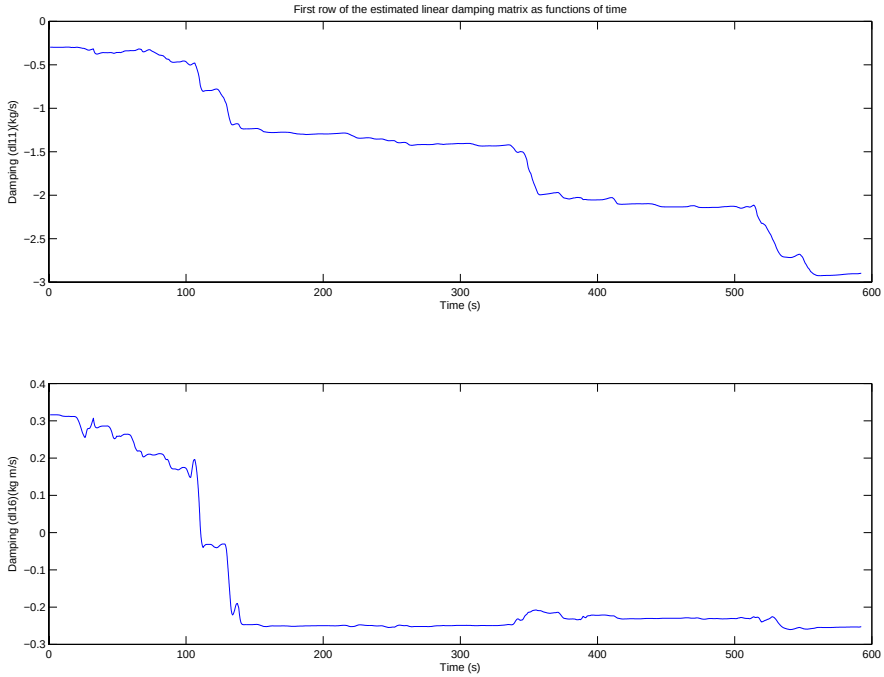

Figure B.5: First row of estimated linear damping matrix as functions of time

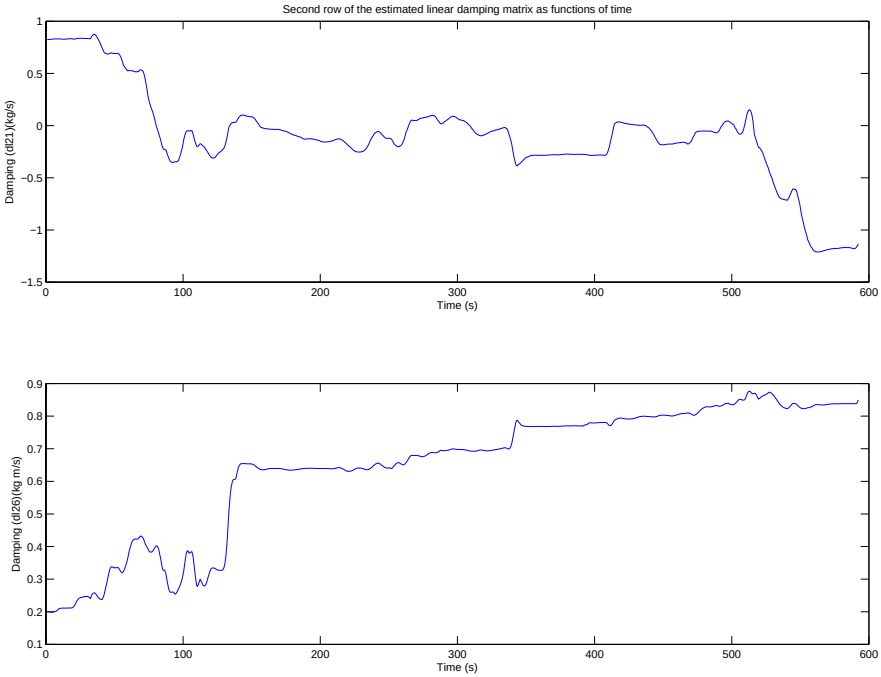

Figure B.6: Second row of estimated linear damping matrix as functions of time

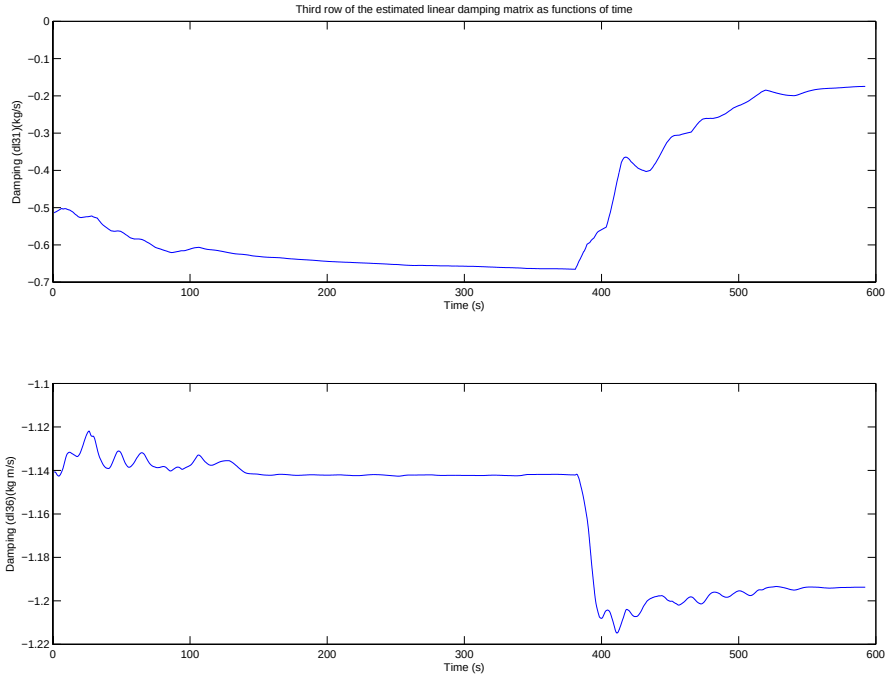

Figure B.7: Third row of estimated linear damping matrix as functions of time

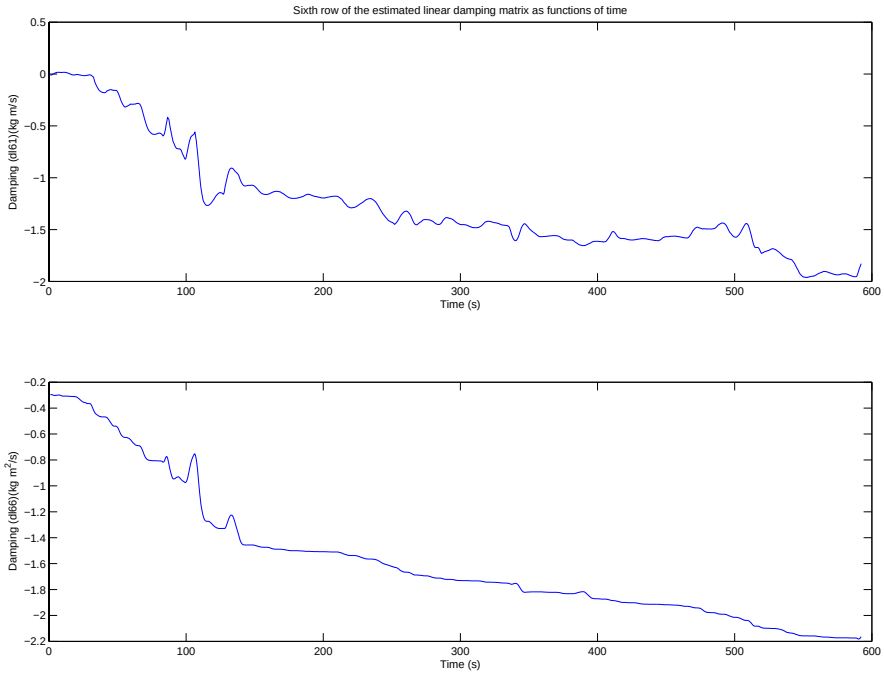

Figure B.8: Sixth row of estimated linear damping matrix as functions of time

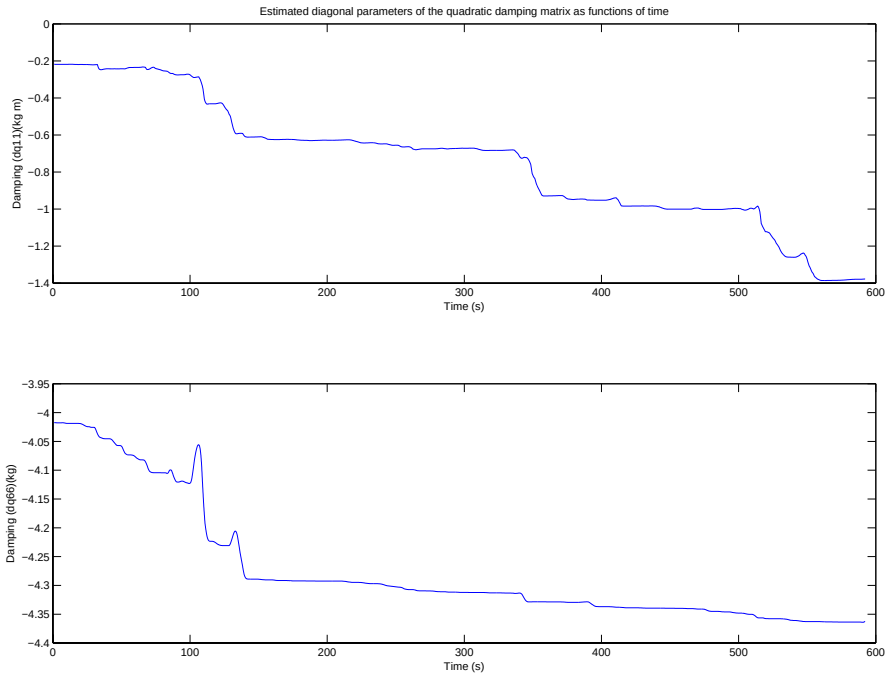

Figure B.9: Diagonal elements of estimated quadratic damping matrix as functions of time

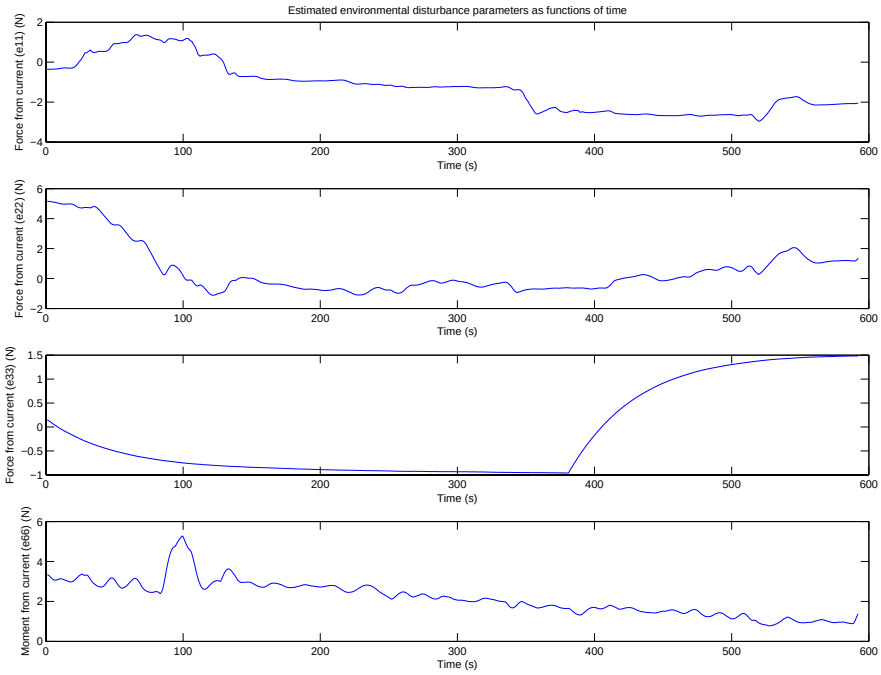

Figure B.10: Estimated environmental disturbance as a function of time

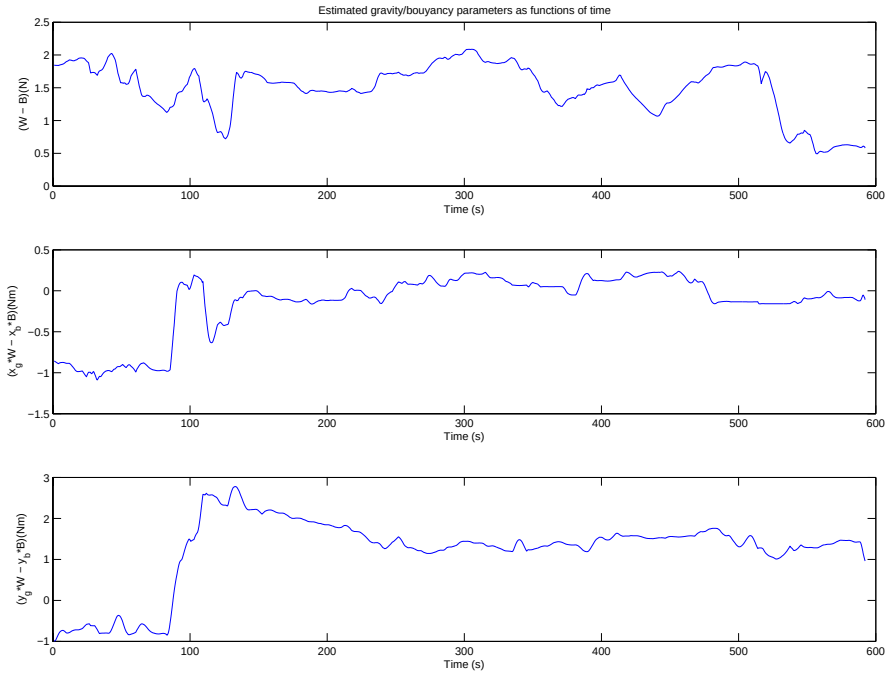

Figure B.11: Estimated gravity/bouyancy parameters as functions of time

Appendix C

Simulator in Matlab/Simulink

The simulator used for the simulations is on the CD-ROM appended to the report. One must first execute the init.m file before running the controlsys.mdl.

Bibliography

L. Daga. Rs232 + str blockset, 2006. URL `http://digilander.libero.it/LeoDaga/`.

T. I. Fossen. *Marine Control Systems - Guidance, Navigation, and Control of Ships, Rigs and Underwater Vehicles*. Marine Cybernetics, 2002.

P. A. Ioannou and J. Sun. *Robust Adaptive Control*. Prentice-Hall, 1996.

M. Ludvigsen and Ø. Ødegaard. *Sammenfatning av hydrodynamiske forsøk med ROVen Minerva*. 2006.

J.-J. E. Slotine and W. Li. *Applied Nonlinear Control*. Prentice Hall, 1991.

Ø. Smogeli and A. J. Sørensen. *Propulsion Control - Lecture slide from course TMR4240 Marine Control Systems*. 2006.

E. Svendby. *Robust Control of ROV/AUVs*. Project report, 2006.

A. J. Sørensen. *Marine Cybernetics - Modelling and Control Lecture Notes UK-2005-76*. 2005.